Integrated graptolite-conodont biostratigraphy and organic carbon chemostratigraphy of the Llandovery of Kallholn quarry, Dalarna, Sweden

Natalia Walasek[a]*, David K. Loydell[a], Jiří Frýda[b], Peep Männik[c], Robert F. Loveridge[a]

[a]School of Earth and Environmental Sciences, University of Portsmouth, Burnaby Road, Portsmouth, PO1 3QL, UK

[b]Faculty of Environmental Sciences, Czech University of Life Sciences Prague, Kamýcká 129, 165 21, Praha 6 and Czech Geological Survey, Klárov 3, 118 21 Praha 1, Czech Republic

[c]Institute of Geology, Tallinn University of Technology, Ehitajate tee 5, 19086 Tallinn, Estonia

* Corresponding author.

E-mail addresses: natalia.walasek@port.ac.uk (Natalia Walasek), david.loydell@port.ac.uk (David K. Loydell), bellerophon@seznam.cz (Jiří Frýda), peep.mannik@ttu.ee (Peep Männik), robert.loveridge@port.ac.uk (Robert F. Loveridge)

ABSTRACT

A revised graptolite and conodont biostratigraphy together with new organic carbon isotope data for the middle Aeronian to lower Telychian (Llandovery, lower Silurian) of Kallholn quarry, central Sweden, are presented. The base of the section is marked by an unconformity between the Ordovician Boda Limestone and Aeronian shales with limestone nodules belonging to the *Pribylograptus leptotheca* Biozone. These are overlain by strata assigned to the lower *Lituigraptus convolutus* Biozone. The *Stimulograptus sedgwickii* Biozone, previously recorded from the section, is absent and marked by an unconformity which is overlain by radiolarian-rich graptolitic shales belonging to the *Stimulograptus halli*

Biozone. The overlying Telychian strata are assigned to the *Spirograptus guerichi*, *Spirograptus turriculatus* and *Streptograptus crispus* biozones. Conodonts indicate that the boundary between the *Distomodus staurognathoides* Biozone and *Pterospathodus eopennatus* Superzone lies within the *Sp. turriculatus* Biozone, as it does also in the Ohesaare core, Estonia. The $\delta^{13}C_{org}$ record shows mostly minor fluctuations but with a distinct twin-peaked positive excursion in the upper *Sp. turriculatus* Biozone, close to the boundary with the overlying *Streptograptus crispus* Biozone. The excursion in the Kallholn section may correlate with the earliest positive shift in $\delta^{13}C$ values at the onset of the excursion associated with the Valgu Event or it may represent a new excursion (provisionally named the Kallholn excursion) preceding this. Many more bentonites (36) occur in the section than previously recorded – geochemical studies are needed to confirm whether the Osmundsberg bentonite (which may or may not be equivalent to the "O" bed in Estonia and Latvia) is present.

Keywords: Silurian; Valgu; Carbon isotopes; Siljan Ring

1. Introduction

The Siljan Ring area of south-central Sweden exposes several sections through graptolitic Silurian strata. Despite a very long history of geological research in the region, dating back to the eighteenth century (Tilas, 1740; see Hedberg, 1988), and recent studies on chemically isolated graptolites from carbonate nodules (e.g. Loydell and Maletz, 2004), detailed graptolite biostratigraphical work has not been published since Törnquist's work in the late nineteenth century. The aims of the present paper are to present a graptolite biostratigraphy for the Llandovery strata (Kallholn Formation) of the northern Kallholn quarry entrance section, Sweden and to integrate this with new conodont biostratigraphical data

from the section. In addition, new $\delta^{13}C_{org}$ data a re presented and these are discussed in relation to the positive carbon isotope excursion (Munnecke and Männik, 2009) associated with the Valgu Event, an interval of turnover in conodont faunas (Männik, 2007). We will also discuss the Osmundsberg K-bentonite, initially identified at Kallholn by Bergström et al. (1998).

2. Locality details and geological background

The Siljan region (Fig. 1) was part of the Baltica palaeocontinent during the Early Palaeozoic. As a result of the closure of the Iapetus Ocean, Baltica and Avalonia collided with Laurentia during the Silurian in a series of complex events comprising the Caledonide Orogeny (Torsvik and Cocks, 2013). Baltica at this time was located in the Southern Hemisphere at a tropical palaeolatitude (Fig. 2) (Torsvik and Cocks, 2013). Eustatic sea-levels were fluctuating, almost certainly as a result of the expansion and contraction of Gondwanan icesheets (Loydell, 1998). Volcanic ashfall deposits (K-bentonites), found in Baltoscandia (including the Kallholn section; e.g. Bergström et al., 1998) and in other parts of Northern Europe originated from explosive eruptions from silicic magma chambers related to subduction along the Iapetus margin (Huff et al., 1998).

According to Baarli et al. (2003, fig. 6), and using Brett et al.'s (1993) interpretations of the depths of benthic assemblage (BA) depths, during the late Aeronian (stated to be *Stimulograptus sedgwickii* Biozone) Kallholn was within BA5 (= depths in excess of c. 50 m), although water depth would presumably vary depending upon proximity to the Boda mounds. We demonstrate below, however, that the *St. sedgwickii* Biozone is not present at Kallholn. Baarli et al.'s palaeogeographical reconstruction is, therefore, almost certainly more reflective of the latest Aeronian *Stimulograptus halli* Biozone than the *St. sedgwickii* Biozone. Baarli et al. (2003) showed shallowing of the Kallholn area in the early Telychian, with water depths (from Brett et al., 1993) of perhaps 30–40 m (BA3) shown for the

Spirograptus turriculatus Biozone. The Siljan region as a whole has been a site of hydrocarbon recovery and exploration since at least the eighteenth century (Hedberg, 1988) and activity in this field continues (see references in Lu et al., 2017).

Kallholn is located within the largest impact crater (75 km diameter) in western Europe, the Siljan impact crater, which has been dated to the Frasnian (Late Devonian), 377 ± 2 Ma (Reimold et al., 2005), recalibrated to 380.9±4.6 Ma by Jourdan et al. (2012). The depression surrounding the central uplift is partially filled by lakes and exposes an up to 10 km wide outcrop of Ordovician and Silurian strata. The Siljan impact structure has recently been drilled and cored as part of the Swedish Deep Drilling Program (see e.g. Lehnert et al., 2012).

The Kallholn (N) section studied (61° 10' 1'' N, 14° 42' 39'' E) exposes a stratigraphical thickness of approximately 15.0 m and is located on the northern side of the entrance road to Kallholn quarry in the northeast of the Siljan area, c. 260 km northwest of Stockholm, Sweden (Fig. 1C). Kallholn quarry lies to the east of regional road 296, northeast of the town of Orsa. A comparable section (Kallholn (S)) occurs on the south side of the entrance road, but is rather overgrown by vegetation. The base of the studied section is marked by an unconformity between limestones of the Hirnantian (Upper Ordovician) Upper Boda Member (part of the Boda Limestone mound facies) and the Silurian Kallholn Formation (Fig. 3; Ebbestad et al., 2015). The 40–50 m high Boda mound at Kallholn is flat-lying, heavily fractured and displays post-depositional karstic fissures up to 25 m deep infilled with graptolitic Llandovery strata (Thorslund and Jaanusson, 1960; Ebbestad et al., 2015; Fig. 5F). The karstic fissures are interpreted to have developed following a fall in sea level of 80–130 m resulting from the Hirnantian glaciation (Kröger et al., 2015).

3. Previous work on the Silurian of Kallholn quarry

The Silurian of the Kallholn quarry entrance road sections (particularly Kallholn (S)) has been studied from a number of different perspectives, including the exceptionally preserved isolated graptolites from dissolved nodules (Loydell, 1991a; Loydell and Maletz, 2004, 2009), chitinozoan biostratigraphy (Grahn, 1998) and correlation of K-bentonites (e.g. Bergström et al., 1998). By contrast with the Ordovician Boda Limestone, however, which has been the subject of numerous papers (see Ebbestad et al., 2015 and references therein), the Silurian has been much less studied in recent years.

The pioneering work on the Silurian of the Kallholn area was undertaken by Törnquist (1874, 1879) and several graptolite species were subsequently described from Kallholn by him (e.g. Törnquist 1890, 1892, 1907). Thorslund and Jaanusson (1960) described the Kallholn quarry as a 'large quarry in the central part of a Boda limestone lentil'. They recorded dark, often somewhat calcareous shales, dating particularly to the *Pribylograptus leptotheca* Biozone, infilling fissures within the limestone. No section through the Llandovery was described, however.

Locality details and a log of the section were provided by Bergström et al. (1998) and the same log was used by Inanli et al. (2009); however, in the absence of prior detailed studies, the graptolite biozonation that they used was highly tentative. The thickness of the Kallholn (S) section was measured as more than 21 m by Bergström et al. (1998), as 18.80 m by Grahn (1998), and subsequently as 18 m by Maletz (in Loydell and Maletz, 2009). This compares with the ~15.0 m recorded in this study in the Kallholn (N) section. Whilst it is possible to correlate Bergström et al.'s (1998) log with that in Figure 3 herein (with the bentonite-limestone-bentonite at around 5 m being a particularly useful marker; we refer to this as the '5 m limestone' below), Grahn's log is highly diagrammatic, although Bergström et al. (2008) were in no doubt that the section studied by Grahn and by them were one and the same.

Loydell (1991a) described a diverse assemblage of isolated graptolites from the *P. leptotheca* Biozone (assigned then to the broadly equivalent *Monograptus argenteus* Biozone) from nodules from the lower 2 m of the section. Bates and Kirk (1984, 1992)

described ancorate biserial graptolites from the same nodules. Maletz (2003) and Loydell and Maletz (2009) described isolated graptolites from the lower *Lituigraptus convolutus* Biozone from an ex situ nodule – the source of this can now be determined as from the 3.93–4.26 m interval.

Grahn (1998) presented biostratigraphical ranges of chitinozoans from the Kallholn (S) section. He suggested that strata from the middle of the section could be assigned to the *Oktavites spiralis* graptolite Biozone, illustrating *Ramochitina nestorae* from this stratigraphical level and the Aeronian biozonal index taxon *Conochitina alargada* from the base of the section. Based on our graptolite biostratigraphy below, it seems very unlikely indeed that the *Oktavites spiralis* Biozone is exposed in the Kallholn sections and especially from the level from which Grahn's illustrated specimen of *R. nestorae* was collected.

Bergström et al. (1998) recorded ten bentonites (5 mm to 25 cm thick) from the Kallholn section from strata assigned provisionally to the *Coronograptus gregarius* (=*Demirastrites triangulatus* to *P. leptotheca*) to *Sp. turriculatus* biozones. The Osmundsberg K-bentonite was originally correlated with the uppermost bentonite (25 cm thick) at Kallholn at 21 m from the base of the Silurian, i.e. near the top of the Kallholn (S) section, but this correlation was subsequently retracted (Inanli et al., 2009). A radio-isotopic age of 437.8 ± 0.5 Ma has been yielded from zircons from this bentonite (Bergström et al., 2008). The precise biostratigraphical level of this bentonite was and remains uncertain.

4. Methods

The samples used in this study were collected during two field excursions (comprising four field days each) in August 2013 by DKL and RFL and in August 2014 by NW, DKL and RFL. During the initial visit the section was logged and graptolites collected in order to establish a biostratigraphical framework for the proposed isotope and palynological analyses. Bentonites and lithological samples were also collected. The main focus of the

second visit was on levels that required higher resolution sampling or to attempt to establish biozonal boundaries more precisely. Levels of particular interest sampled at closer intervals of 5 cm included those at the base of the section, shales surrounding a flat-topped nodule at 4.26 m, the distinct limestone bed at 5.0 m, shales at 9–10 m and the uppermost two metres of the section.

Excavation of the section was required where exposure was poor and at levels where the shales had weathered and were overlain by scree or soil. This was at base of the section of up to 0.85 m, between 5.26 m and c. 8 m and above c. 10 m. It was difficult and dangerous to collect from the Kallholn (N) section between 3.8 m and 4.2 m and therefore the easily correlated discontinuous shale sandwiched between two conspicuous layers of nodular limestones was sampled from the Kallholn (S) section.

The number of graptolites collected from each horizon reflects their abundance and ease of collection, together with effort expended on horizons of perceived significance. Graptolites were studied and identified largely using a binocular microscope and photographed using a Leica EZ4 HD USB microscope. A small number of isolated graptolites from low in the section were examined using the SEM (Zeiss EVO/MA10). Approximately 3,300 graptolites were examined and 2,780 were identified to species level. Other graptolites were identified only to genus level due to their incompleteness and/or orientation on the rock surface. Figured graptolites are housed at the Museum of Evolution, Uppsala University, Sweden.

Limestone nodule samples from five horizons (7.29–7.49 m, 8.70–8.80 m, 13.66–13.91 m, 14.73–14.82 m and 14.76–14.91 m) were processed for conodonts. All samples were dissolved in buffered acetic acid. After this procedure, residues were treated with buffered formic acid (following the method by Jeppsson and Anehus, 1995) to dissolve dolomite. Insoluble residues were washed using the decanting method (no sieving) and, after drying at room temperature, picked under a binocular microscope. Weight of the samples varied between 0.17 and 0.75 kg. All samples except that from 7.29–7.49 m were productive. In total 105 identifiable conodont specimens were recovered. Preservation of the specimens

196 is variable, most of them are broken. The colour of conodonts is pale yellow (CAI = 1 of
197 Epstein et al., 1977). Selected specimens were studied and photographed using the SEM
198 (Zeiss EVO/MA15). Figured conodonts are housed at the Institute of Geology, Tallinn
199 University of Technology (collection number GIT 793).
200 For organic carbon isotope analyses hand specimens were cut and rock powder was
201 prepared from a few grams of fresh sample. Before analyses, rock powders were
202 decarbonatized with 6 N HCl at 40°C for several hours, then washed and dried. Insoluble
203 fractions were then repeatedly rinsed in ultrapure water and dried at 80°C. About 10 mg of
204 rock powder were used for each isotope analysis. Samples were combusted in a Fisons
205 1108 elemental analyser (ThermoScientific) coupled on-line to Thermo Delta 5 mass
206 spectrometer via a ConFlo interface. NBS 22 (Gulf oil, with $\delta^{13}C$ value -29.75‰) was used
207 as a reference material. Accuracy and precision were controlled by replicate measurements
208 of laboratory standards and were better than ±0.1‰ (1σ).
209
210
211 **5. Description of the Kallholn (N) section**
212
213 The approximately 15-m-thick section is composed primarily of shale. Carbonate
214 nodules, which vary in size from a few millimetres to a few metres in diameter, are common
215 in the *P. leptotheca*–lower *L. convolutus* biozones (Fig. 4D) but become much less frequent
216 at higher levels (Fig. 4C). They indicate numerous brief intervals of non-deposition (Raiswell,
217 1987). Comparable nodules, from Osmundsberget, have been studied in detail by Morad
218 and Eshete (1990). A detailed sedimentological analysis of the rocks in the section is beyond
219 the scope of this work – we focus here on the dominant lithologies and key marker beds.
220 Both the lithologies and the fossil assemblages at Kallholn indicate fluctuations between oxic
221 (bioturbated, e.g. at 14.3 m), dysoxic (shales with *Chondrites* and/or pyrite filled/lined
222 burrows) and anoxic conditions (unbioturbated black shales) (Fig. 5H). Recent geochemical

analyses of samples from cores drilled through the Kallholn Formation in the Siljan area have also indicated fluctuating bottom water oxicity during its deposition (Lu et al., 2017). Benthic organisms are generally rare throughout the section and are in some cases clearly allochthonous, with storms likely to have been responsible for numerous limestone beds (predominantly below the 5.21 m level) which vary in thickness laterally, e.g. the crinoidal limestone at 3.86 m (Fig. 5A).

The base of the section (0–0.85 m; Fig. 4D) consists of poorly exposed shales with better exposed nodules which in some cases appear to be cemented to the unconformity. At this level and elsewhere in the lower part of the section some of the nodules have been rotated (laminations within them are at an angle to those within shales) probably as a result of the meteorite impact, as previously commented upon by Loydell and Maletz (2009). Overlying strata are well exposed and consist of further shales and nodules, one of which is 0.3 m thick and 1.55 m wide. Several thin (5–20 mm) limestones occur between 2.18 m and 3.26 m. A highly irregular (nodular) limestone unit occurs from 3.91 m to 4.26 m with a distinctly flat-topped (planed-off) nodule (Fig. 5B–D) at the top (marking an unconformity between the *L. convolutus* and *St. halli* biozones). This limestone contains pockets of shale in its central part, between the nodules. It is more safely examined in the Kallholn (S) section. Overlying the unconformity are black shales which in polished and thin sections can be seen to contain abundant radiolarians (Fig. 5B, C). Lower Silurian radiolarians have previously been recorded from the Scandinavian Platform by Maletz and Reich (1997), Noble and Maletz (2000) and Umeda and Suzuki (2005). A low-angle fault occurs between the unconformity and a very useful marker bed (Fig. 5E), a thin limestone (10 mm thick) at 4.57 m, the latter being present also in the Kallholn (S) section. Logging of this unfaulted Kallholn (S) section demonstrates that the fault cuts out about 0.54 m of strata on the north side, all within the *St. halli* Biozone.

Bentonites are rare in the demonstrably Aeronian part of the section (below 4.98 m), with only two present (at 3.47 m and 4.31 m). A distinct marker bed within the section is a limestone bed (with a varying thickness of 16–21 cm; Fig. 4B) with its base 5 m from the

bottom of the section, with bentonites directly below and above. This marker bed enables correlation with the log published by Bergström et al. (1998) and reproduced in Inanli et al. (2009) which also shows a limestone at the 5 m level with immediately under- and overlying bentonites.

The section is poorly exposed (except for nodules) between 5.26 m and 8.0 m. The sediment is glauconitic at 6.41-6.46 m, which, along with absence of graptolites may indicate shallowing or washed in material. Dark grey shales, in some cases rusty weathering, dominate throughout the upper part of the section being well exposed at c. 8–10 m but poorly exposed above c. 10 m. *Chondrites* occurs in the black shales at 10.92–11.10 m and 12.05 m. Pyrite is commonly found in the higher parts of the section in layers (10.80 m) and nodules (e.g. at 9.79 m and 10.12 m). Above c. 10.0 m there is a noticeable alternation of black and paler shales with common thin (10–30 mm thick) bentonites (Fig. 4E).

Cone-in-cone structures are present within the cemented layer at 11.79 m providing evidence for early diagenesis (Fig. 5F) (Buchardt and Nielsen, 1985). Two large nodules are present near the top of the section (Fig. 4C) at 13.66 m (25 cm thick and 95 cm wide) and 14.61 m (30 cm thick and 60 cm wide). The 13.66 m nodule displays recrystallization of micrite into microspar (Fig. 5G) such as has previously been observed within carbonate concretions from the Lower Rastrites Shales (= Kallholn Formation) at Osmundsberget (Morad and Eshete, 1990).

Graptolites are present throughout much of the section within the shales and some of the carbonate nodules. Within the shales they are mainly preserved flattened, less commonly as pyrite internal moulds; three-dimensional preservation of graptolites (as described by Loydell, 1991a and Loydell and Maletz, 2009) is found in some of the nodules. Graptolites were most abundant in the lower *P. leptotheca*, lower *Sp. turriculatus* and *Streptograptus crispus* biozones, with the least abundant assemblages (less than ten identifiable specimens) around the *P. leptotheca*/*L. convolutus* Biozone boundary and in the middle to upper *Sp. turriculatus* Biozone. Other fossils found within the section include

lingulate brachiopods, articulate brachiopods (especially small strophomenids), pelmatozoan columnals, and rare trilobites, ostracods and bivalves.

6. Graptolite biostratigraphy of the Kallholn (N) section

Stratigraphical ranges and relative abundances of all taxa collected are presented in Figure 6. The total number of species (including those left in open nomenclature) identified is 90. Six biozones have been recognised in the Kallholn (N) section: *Pribylograptus leptotheca*, *Lituigraptus convolutus*, *Stimulograptus halli*, *Spirograptus guerichi*, *Spirograptus turriculatus* and *Streptograptus crispus.* Biostratigraphically important taxa are illustrated in Figures 6–9.

The *P. leptotheca* Biozone comprises the lower 3.78 m of Silurian strata, which unconformably overlie the Ordovician Boda Limestone. The biozone is characterized here, particularly in its lower part where assemblages are almost monospecific, by a high abundance of *C. gregarius* (Fig. 7A) with siculae 6–10.5 mm long. The highest abundances were recorded at 1.25 m (91 specimens) and 1.33–1.38 m (176 specimens). Hutt (1975) recorded *C. gregarius* with siculae 4.5-6.3 mm long from the *D. triangulatus* and *Neodiplograptus magnus* biozones, with longer siculae occurring only within the *P. leptotheca* Biozone (a feature noted also by Štorch, 1998). The lowermost Kallholn sample included a specimen of *C. gregarius* with a sicula at least 7 mm long. Further evidence that the lower part of the section, below the first appearance of *P. leptotheca* in the 1.13–1.18 m sample, belongs in the *P. leptotheca* Biozone comes from the presence of *Monograptus* aff. *imago sensu* Štorch (1998) (Fig. 8A) which appears at 0.70 m. This species has not been recorded from below the *P. leptotheca* Biozone in the Tmaň section Bohemia (Štorch, 1998). *P. leptotheca* (Fig. 8D) is most abundant at 1.56–1.60 m, with 73 specimens recorded. Other typical *P. leptotheca* Biozone species found at Kallholn include *Agetograptus primus* (Fig.

8J), *Campograptus millepeda* (Fig. 8I), *Coronograptus maxiculus* (Fig. 8E), '*Monograptus*' *havliceki* (Fig. 8F), *Rastrites longispinus* (Fig. 8G) and *Lituigraptus richteri* (Fig. 8C).

The *L. convolutus* Biozone is represented in only one sample (3.93–3.98 m) in the Kallholn (N) section in which *Torquigraptus denticulatus* (Fig. 7B) and *Metaclimacograptus minimus* occur. *L. convolutus* occurs in the Kallholn (S) section in black shales between the two distinctive nodular limestone layers easily correlated into the (N) section (where they occur between 3.91 m and 4.26 m). The presence also of *Campograptus lobiferus* (Fig. 8K), '*Monograptus*' *inopinus* and *Rastrites approximatus* (Fig. 8B) indicates the lower part of the *L. convolutus* Biozone for this black shale intercalation.

The absence of the *St. sedgwickii* Biozone from the section is the result of an unconformity, at 4.26 m, between the *L. convolutus* and *St. halli* biozones which is marked by the flat-topped (upper part planed off by erosion) carbonate nodule referred to above (Fig. 5B–D).

The appearance of *St. halli* (Fig. 7C) indicates the *St. halli* Biozone at 4.26 m. This, however, is not necessarily the biozone's true base due to the underlying unconformity, but the absence of *Lituigraptus rastrum* at this level (and presence higher up; Fig. 6) does indicate the lowest subzone of the *St. halli* Biozone (Loydell et al., 2015). Other species present within the biozone, occurring above the limestone at 4.57 m, include *Lituigraptus bostrychodes* (Fig. 9D), *St. sedgwickii, Parapetalolithus mui* (Fig. 8H), *L. rastrum* (Fig. 9A), *Parapetalolithus kunkojensis, Pristiograptus variabilis, Torquigraptus linterni* and *Rastrites schaueri* (Fig. 9B). The presence of *L. rastrum* (a subzonal index graptolite for the middle of the *St. halli* Biozone; Loydell et al., 2015) in the highest graptolitic sample below the 5 m limestone indicates that the upper part of the *St. halli* Biozone is not represented by graptolitic strata (if at all) in the section.

The limestone at 5.0 m yielded no graptolites and therefore may be of either latest Aeronian or earliest Telychian age. The first occurrence, at 5.26 m, of *Streptograptus* species (*Streptograptus dalecarlicus* (Fig. 7D) and *Streptograptus filiformis*) together with '*Monograptus*' *gemmatus* (Fig. 9C), marks the base of demonstrably Telychian strata. The

Sp. guerichi Biozone is represented by 3.03 m of strata ranging from 5.26 m to 8.29 m. Graptolites are not common and are mostly fragmentary through this poorly exposed part of the section.

Other species present within the *Sp. guerichi* Biozone include *Streptograptus pseudoruncinatus* and *Sp. guerichi. 'M.' gemmatus*, a useful marker for the lower to middle *Sp*. *guerichi* Biozone, is found between 5.26 m and 6.43 m. The upper part of the *Sp. guerichi* Biozone is marked by the first appearance of *Torquigraptus planus* (Fig. 9G) at 6.86 m.

The *Sp. turriculatus* Biozone is the thickest biozone exposed in the section spanning from 8.29 m to 14.16 m. Its base is recognised by the first appearances of *Sp. turriculatus* (Fig. 9I) and *Streptograptus johnsonae* (Fig. 9E). The lower to middle part of the biozone displays a very consistent assemblage with very abundant *S. johnsonae* together with common *Sp. turriculatus*, *Pristiograptus bjerringus* (Fig. 9H), *Parapetalolithus altissimus, Streptograptus tenuis* (Fig. 7F), *Streptograptus whitei* (Fig. 7G), *'Monograptus' tureki* (Fig. 7I) and *Monograptus marri*. The highest occurrence of *S. johnsonae* is at 10.8 m. *Torquigraptus proteus* (Fig. 7H) first appears at 10.54 m indicating the upper part of the *Sp. turriculatus* Biozone.

The first appearance of C*ochlograptus veles* (Fig. 9F) at 14.16 m is taken here to define the base of the *S. crispus* Biozone. Its first appearance coincides with that of *S. crispus* in Britain (Zalasiewicz, 1994) and is above the FAD of *S. crispus* in Bohemia (Štorch 1994). There is an absence of identifiable graptolites for 0.35 m below the first occurrence of *C. veles* at Kallholn. The *S. crispus* Biozone is represented by 0.79 m of strata ranging up to the top of the section. Other taxa recorded from this biozone include *T. proteus* and abundant *Stimulograptus clintonensis*. The presence of *Streptograptus pseudobecki* at 14.77–14.79 m and 14.85–14.90 m indicates that the section ends in the lower part of the *S. crispus* Biozone as this species has not been recorded from higher stratigraphical levels (Loydell, 1990).

Our graptolite biozonation is thus significantly different from the 'provisional' version provided by Bergström et al. (1998) for the Kallholn (S) section (Fig. 3). Bergström et al. (1998) assigned strata below the 5 m limestone to the *C. gregarius* Biozone (=*D. triangulatus*– *P.leptotheca* biozones) representing the lower half of the Aeronian, whereas we demonstrate that these beds represent the *P. leptotheca*, lower *L. convolutus* and lower–middle *St. halli* biozones. Above the 5 m limestone the beds were assigned by Bergström et al. (1998) to the upper Aeronian *St. sedgwickii* Biozone, a biozone that is not present at all in the section (there is an unconformity at this level), whereas these beds are shown herein to be entirely of Telychian age. The highest beds in the Kallholn (S) section are shown by Bergström et al. (1998) to be within the *Sp. turriculatus* Biozone. Bergström et al. (1998) logged a greater thickness (more than 21 m) in the Kallholn (S) section. Examination by us of this now rather overgrown and in parts poorly exposed section indicated that there is indeed a greater thickness of strata above the 5 m limestone here than in the Kallholn (N) section, but the overall thickness of the section was less than 21 m (and appeared much closer to the 18 m measured by Maletz, in Loydell and Maletz, 2009), so it is possible that the thick bentonite originally identified by Bergström et al. (1998) as the Osmundsberg bentonite (at 21 m) is no longer exposed. The age of the highest beds exposed in the Kallholn (S) section remains to be established.

7. Conodont biostratigraphy of the Kallholn (N) section

Selected conodonts from the Kallholn (N) section are illustrated in Figure 10, with the distribution of identified taxa shown in Figure 6. The lowest of the samples processed (7.29–7.49 m) yielded no conodonts. That from 8.70–8.80 m yielded a *Distomodus staurognathoides* Biozone assemblage including *D. staurognathoides* (Fig. 10A), *Oulodus*? sp. (Fig. 10B,C), *Aspelundia*? *fluegeli* (Fig. 10D–G) and *Dapsilodus* sp. (Fig. 10H,I). The higher samples (13.66–13.91 m, 14.73–14.82 m and 14.76–14.91 m) are all from the

Pterosphathodus eopennatus Superzone, but the fragmentary nature of the rare specimens of *Pt. eopennatus* (Fig. 10J,M,N,R) precludes assignment to either of its biostratigraphically significant subspecies. The presence of *Astropentagnathus irregularis* (Fig. 10K,Q,S,T) in the highest sample indicates that this must be from below Valgu Event Datum 2 (at which *A. irregularis* becomes extinct; Männik, 2007) and therefore from the *Pt. eopennatus* ssp. n. 1 Biozone. Also present in all three of the higher samples is *Dapsilodus* aff. *sparsus* (Fig. 10L,O,P). Clearly the *D. staurognathoides/Pt. eopennatus* ssp. n. 1 biozonal boundary must lie between 8.8 m and 13.66 m and thus is within the *Sp. turriculatus* Biozone as it was shown to be in the Ohesaare core, Estonia (Loydell et al., 1998).

8. Bentonites

In our study, 36 bentonites have been recorded (Fig. 3), varying in thickness from 1 mm to 6 cm. This is substantially more than the ten bentonites recorded by Bergström et al. (1998). No bentonites were found in the lower 3.47 m of the section (*P. leptotheca* Biozone); they become more frequent in the upper part of the section above 4.98 m. The difference in bentonite thicknesses (much thinner) in our log compared with those shown by Bergström et al. (1998) may be the result of gravitational compression of the soft bentonitic material between harder layers. The bentonite was simply ‘squeezed’ out and weathered away from the edge of the exposure.

Our new graptolite biostratigraphy of the Kallholn (N) section provides some indication of where the Osmundsberg K-bentonite might be located here. This bentonite is 1.15 m thick (Bergström et al. 1998) at its type locality, Osmundsberget, only 30 km southeast of Kallholn. Following work on the graptolites at Osmundsberget by Loydell and Maletz (2002, 2004), in which a lower *Sp. turriculatus* Biozone assemblage including *S. johnsonae* was recorded from carbonate nodules less than 0.5 m below the bentonite, Bergström et al. (2008, 2012) reasonably enough placed the Osmundsberg K-bentonite in

416 the lower part of the *Sp. turriculatus* Biozone. Bergström et al. (2012) assigned a low
417 diversity assemblage of conodonts from the highest level to yield them in the
418 Osmundsberget section, 0.5 m below the Osmundsberg K-bentonite, to the *D.*
419 *staurognathoides* Biozone.
420 Bergström et al. (1998) originally identified the 0.25 m thick bentonite (SWE 132) 21
421 m above the base of the Silurian in the Kallholn (S) section as the Osmundsberg K-
422 bentonite, but subsequently Inanli et al. (2009) noted significant geochemical differences
423 between SWE 132 and the Osmundsberg K-bentonite and the two are no longer considered
424 to be correlative, although Huff (2016, fig. 13) shows them as such. This is consistent also
425 with the differing radiometric ages provided by the two bentonites: the Osmundsberg K
426 bentonite from Osmundsberget was dated as 438.7±1.0 Ma by Bergström et al. (2008)
427 whereas a rather younger age (437.8±0.5 Ma) was provided by SWE 132 from Kallholn (S).
428 We have identified 18 bentonites within the *Sp. turriculatus* Biozone in the Kallholn (N)
429 section: future geochemical analyses may identify one of these as the Osmundsberg K-
430 bentonite.
431 The Osmundsberg K-bentonite has been widely recognised elsewhere on Baltica and
432 particularly in Estonia where it is referred to as the “O” bed (Kiipli et al., 2001). Here it is 10–
433 25 cm thick and occurs in the Rumba Formation. Kiipli et al. (2001) stated that it can be
434 confidently distinguished from all other bentonites based on its low Nb content (3–11 ppm;
435 Kiipli et al., 2001, tables 1 and 2). Huff et al. (1998, table 1) recorded 12–14 ppm Nb in their
436 analyses of the Osmundsberg K-bentonite from Osmundsberget. Interestingly, bentonite
437 SWE 132 from Kallholn, which was originally considered to be the Osmundsberg K-
438 bentonite, but subsequently (Inanli et al., 2009) shown to be significantly different in its
439 geochemistry, also has low Nb (12 ppm; Huff et al., 1998), suggesting that more than one
440 ash erupted in the early Telychian has this geochemical signature. Also of note is the fact
441 that one of the beds that Inanli et al. (2009) did identify “with a high degree of confidence” as
442 the Osmundsberg K-bentonite based on its geochemistry, DL3, from Dob’s Linn, Scotland is
443 from the upper Aeronian rather than lower Telychian. Loydell (1991b) demonstrated that the

level of DL3 was within the *St. halli* Biozone. Thus it appears that ashes from different eruptive events can have a very similar geochemical signature. Before attempting chemostratigraphical correlation, be it using bentonites or isotopes, the biostratigraphy must be carefully considered.

It is also worth noting that the "O" bed in Estonia is described as a yellow hard feldspathite by Kiipli et al. (2001) and this is true of both core and outcrop samples. The Osmundsberg K-bentonite of Osmundsberget is, by contrast, a soft clay which disaggregates readily during wet sieving (Huff et al., 1998). Whether the Osmundsberg K-bentonite and "O" bed are the products of the same eruption is clearly significant for correlation across Baltica and beyond.

Kiipli and Kallaste (2002) identified the "O" bed in the Aizpute-41 core, Latvia at a depth of 964.4 m. Loydell et al. (2003) recorded from the same core *Sp. turriculatus* Biozone graptolite assemblages, including *T. proteus*, from 964.58 m and 964.62 m, with *S. johnsonae* occurring also in the lower of the two core samples. At Kallholn the ranges of these two species overlap between 10.54 m and 10.8 m, suggesting that the "O" bed should be sought in samples from this interval or higher at Kallholn.

9. The $\delta^{13}C_{org}$ record

The results of $\delta^{13}C_{org}$ analyses for the Kallholn (N) section are presented in Figure 11. A table of the $\delta^{13}C_{org}$ values is presented in Appendix 1. Values range from -30.31 ‰ to -27.33 ‰, both recorded from the *Sp. turriculatus* Biozone. Throughout the majority of the section (up to 12 m) values remain below -29 ‰, characterizing the *P. leptotheca, L. convolutus, St. halli, Sp. guerichi* and lower parts of the *Sp*. *turriculatus* biozones (and also the highest part of the section in the *S. crispus* Biozone).

The lowermost part of the section (0–0.5 m nodule) commences with a $\delta^{13}C_{org}$ value of -29.78 ‰ with a very similar value of -29.74 ‰ from the 0.04–0.13 m nodule. This is

472 followed by a set of clear minor fluctuations (evident from the clusters of data points) within
473 the lower *P. leptotheca* Biozone: values decrease from between -29.87 ‰ and -29.97 ‰
474 (recorded from both carbonate nodules and black shales) at 0.93–1.38 m to between -30.08
475 ‰ and -30.21 ‰ from samples (shales, nodules and a limestone bed) at 1.45–1.65 m. The
476 values increase again to -29.84 ‰ and -29.89 ‰ in the black shales at 1.73–1.98 m then
477 decrease again to values ranging between -30.08 ‰ and -30.10 ‰ in nodules and shales
478 from 2.00–2.18 m. Fluctuations in values above this level have a less regular pattern. The
479 first more pronounced peak of -29.25 ‰ is at 3.53 m (high within the *P. leptotheca* Biozone).
480 Within the *L. convolutus* Biozone, just below the unconformity, values range between -29.74
481 ‰ and -29.78 ‰.
482 Above the unconformity, within the lower-middle *St. halli* Biozone, values show minor
483 fluctuations with the lowest value of -30.16 ‰ at 4.78–4.83 m. Three samples have been
484 analysed from the limestone band at 5.0–5.21 m all showing a distinctive increase in values
485 from -29.43 to -29.01 ‰. Above this minor positive excursion at 5.0 m an interval of low
486 values (ranging from -29.97–30.16 ‰) can be observed through much of the lower *Sp.*
487 *guerichi* Biozone until the values increase to -29.34 ‰ at 6.41–6.46 m. The values continue
488 to fluctuate with no clear trend evident through much of the upper *Sp*. *guerichi* Biozone. The
489 uppermost *Sp. guerichi* Biozone and lowermost *Sp. turriculatus* Biozone are characterized
490 by low values, close to or below -30 ‰. The lowest value (-30.31 ‰) is recorded from black
491 shales at 8.71-8.77 m (lower *Sp. turriculatus* Biozone). Values then increase steadily to -
492 29.18 ‰ in the black shales at 9.36–9.41 m. Between this level and 10.76–10.81 m the
493 values fluctuate between -29.18 ‰ (9.36–9.41 m) and -29.77 ‰ (9.56–9.61 m).
494 Overall, the values start to increase from -29.91 ‰ at 11.13–11.18 m culminating in
495 values of -27.72 ‰ (at both 12.41 m and 12.61 m, from both black shales and a nodule),
496 representing a positive shift of more than 2 ‰. Values fall sharply to ranging from -28.75–
497 29.23 ‰ before a second peak of -27.33 ‰ (again representing a positive shift of
498 approximately 2 ‰) recorded from a nodule at 13.66 m. This pronounced twin-peaked
499 excursion is high in the *Sp. turriculatus* Biozone, close to the boundary with the overlying *S.*

crispus Biozone. The highest part of the section records declining values, with -29.78 ‰ recorded from the penultimate sample from the *S. crispus* Biozone.

9.1 Discussion

Other than the positive excursion close to the to the *Sp. turriculatus/S. crispus* Biozone boundary, the Kallholn $\delta^{13}C_{org}$ values show only minor fluctuations. We discuss below how the $\delta^{13}C_{org}$ curve for Kallholn (N) compares with published curves through the Aeronian and lower Telychian.

9.1.1. Aeronian

Within the Aeronian of Kallholn there is of course no record of the major positive excursion in the *St. sedgwickii* Biozone (Melchin and Holmden, 2006; Štorch and Frýda, 2012) as there is an unconformity at this level. The *P. leptotheca* and lower *L. convolutus* biozones are characterized in the Czech Republic (Frýda and Štorch, 2014) by only minor fluctuations in $\delta^{13}C_{org}$ values, a pattern shown also by $\delta^{13}C_{org}$ curves from Dob's Linn, Scotland and Arctic Canada (Melchin and Holmden, 2006). Differences in sampling density (e.g. 30 samples analysed herein from the *P. leptotheca* Biozone of Kallholn, compared with three from the Radotín tunnel and six from Hlásná Třebaň, Bohemia; Frýda and Štorch, 2014) inevitably affects the comparisons that can be made between sections, as does uncertainty about where within the *P. leptotheca* Biozone the Kallholn record commences. Thus far the very minor positive excursion high in the *P. leptotheca* Biozone at Kallholn (Fig. 11) has not been identified in other sections.

Faulting in the *St. halli* Biozone of the Kallholn (N) section makes direct comparison difficult with the $\delta^{13}C_{org}$ curve through this interval from the El Pintado section, Spain (Loydell

et al., 2015). It is possible, however, that the positive excursion recorded in the 5 m limestone is equivalent to the small positive excursion in the *L. rastrum* Subzone (middle *St. halli* Biozone) recorded by Loydell et al. (2015). This would require there to be another minor unconformity in the Kallholn (N) section (with the upper *St. halli* Biozone missing), as immediately above the bentonite overlying the 5 m limestone the graptolite assemblages indicate the lower Telychian *Sp. guerichi* Biozone. Support for there being a minor unconformity at this level comes also from the absence of a significant negative carbon isotope excursion (the "Rumba low" – see discussion below) within the Kallholn (N) $\delta^{13}C_{org}$ data.

9.1.2. Lower Telychian

A detailed comparison of $\delta^{13}C_{org}$ curves through the *Sp. guerichi* Biozone of El Pintado, Spain and Cape Manning, Cornwallis Island, Arctic Canada was provided by Loydell et al. (2015). The lower part of the biozone is characterized by more negative values and the upper part by less negative values, a trend that is shown also in the Kallholn data (Fig. 11). A brief interval of more negative values characterizes the *Sp. guerichi/Sp. turriculatus* Biozone boundary interval at El Pintado and this correlates biostratigraphically with a similar interval of more negative values between 8.06 m and 9.17 m in the Kallholn (N) section.

Our $\delta^{13}C_{org}$ data show a distinct twin-peaked positive excursion in the upper *Sp. turriculatus* Biozone, close to the *Sp. turriculatus/S. crispus* Biozone boundary with the upper peak at a level assigned to the lower part of the *Pt. eopennatus* ssp. n. 1 conodont Biozone. The lower peak may be in the uppermost part of the *D. staurognathoides* Biozone or in the lower *Pt. eopennatus* ssp. n. 1 conodont Biozone. A positive $\delta^{13}C_{carb}$ excursion commencing at a similar stratigraphical level has previously been recorded on Baltica by Kaljo and Martma (2000) and by Munnecke and Männik (2009) and has been associated with a

conodont extinction event, the Valgu Event of Männik (2007). Subsequently a “Valgu excursion” appeared on the “generalized $\delta^{13}C_{carb}$ curve” for the Silurian of Cramer et al. (2011) and in *The Geologic Time Scale 2012* (Melchin et al., 2012) and has been referred to in several publications on the Llandovery of North America (e.g. McLaughlin et al., 2012; Sullivan et al., 2014; Bancroft et al., 2015; McAdams et al., 2017; Waid and Cramer, 2017).

The positive excursion in the Kallholn (N) section is unusual by comparison with other carbon isotope curves through the lower Telychian in that it has two pronounced peaks (although this may simply reflect the greater density of sampling at Kallholn) followed by a rapid return to pre-excursion values. Determining whether the twin-peaked excursion at Kallholn represents a newly recognised positive excursion (if it is, naming it the Kallholn excursion would seem appropriate) or is part of the excursion associated with the Valgu Event requires examination of the stratigraphical position of the latter, particularly in the core from which it was first described, Viki, drilled on Saaremaa Island, western Estonia.

The Viki core is very interesting in that it records over a very limited depth range within the Rumba Formation (0.4 m, of which 0.1 m was deposited geologically instantaneously) a negative $\delta^{13}C_{carb}$ excursion (with the lowest value, 0.28 ‰, at 185.35 m; Munnecke and Männik, 2009), the “O” bed (bentonite) at 185.1-185.0 m and then the commencement of the positive excursion associated with the Valgu Event, with a value of 1.25 ‰ at 184.95 m. A question that needs to be addressed is whether the suddenness of this positive shift in values might indicate a stratigraphical gap in the Viki core succession, in which case the carbon isotope curve from here may not be a complete record of changes in oceanic chemistry through this part of the Llandovery.

The negative $\delta^{13}C$ excursion has been identified within the Rumba Formation from other sections (e.g. Kirikuküla, Ikla) and has been referred to as the “Rumba low” (Kaljo and Martma, 2000). It appears in both the $\delta^{13}C_{carb}$ and $\delta^{13}C_{org}$ records (Gouldey et al., 2010). Kaljo and Martma (2000) referred the Rumba Formation to the Aeronian, Munnecke and Männik (2009) and Cramer et al. (2011) have it straddling the Aeronian/Telychian boundary, whilst Gouldey et al. (2010) place it entirely within the Telychian. Recognition of the “O” bed

584 towards the top of the Rumba Formation indicates that the uppermost part of the formation
585 must be of Telychian age: as noted above *Sp*. *turriculatus* Biozone graptolites were recorded
586 from below the “O” bed in the Aizpute-41 core, Latvia (Loydell et al., 2003).
587 Evidence for the age of the “Rumba low” comes from the Ikla core from which Kaljo
588 and Vingissaar (1969) recorded *Pseudoclimacograptus* [now *Metaclimacograptus*] *hughesi*
589 from 316.6 m, exactly the same depth as the lowest $\delta^{13}C_{org}$ value of -30.02 ‰ and above the
590 lowest $\delta^{13}C_{carb}$ value of -0.95 ‰ which is at a depth 320.0 m. There are no records worldwide
591 of *Me. hughesi* from the Telychian, but it has been very widely recorded from the
592 Rhuddanian and Aeronian. Conodonts unfortunately provide no useful additional
593 stratigraphical precision for dating the “Rumba low”: conodonts are sparse and the *D.*
594 *staurognathoides* Biozone to which much of the Rumba Formation (including the “Rumba
595 low”) has been assigned (Munnecke and Männik, 2009) extends stratigraphically downwards
596 from the lower Telychian into the lower Aeronian (Loydell et al., 2010). Based on the Ikla
597 graptolite record, it seems reasonable to assign at least part of the “Rumba low” to the
598 Aeronian, with the excursion perhaps straddling the Aeronian/Telychian boundary.
599 Assuming that the negative $\delta^{13}C$ excursions (“Rumba low”) in the Rumba Formation
600 are synchronous in the Ikla and Viki cores, it therefore appears that there must be an
601 unconformity in the Viki Core somewhere between 185.35 m and 185.1 m with at the very
602 least most/all of the *Sp. guerichi* Biozone missing. Such an unconformity would not be at all
603 unusual for Estonia or Latvia: e.g. in the Ohesaare core, also from Saaremaa, much of the
604 Aeronian is missing together with the lower Telychian, the lowest strata above the
605 unconformity being of *Sp. turriculatus* Biozone age (Loydell et al., 1998) and in the Kolka
606 core, northern Latvia, the upper Aeronian and lower Telychian are missing, again with the
607 lowest strata above the unconformity being of *Sp*. *turriculatus* Biozone age (Loydell et al.,
608 2010).
609 Having established that the onset of the excursion involves $\delta^{13}C$ values from samples
610 (one most probably of Aeronian age, the other above a bentonite from the *Sp*. *turriculatus*
611 Biozone) straddling an unconformity that must omit part of the lower Telychian, we now need

612 to consider the biostratigraphical position of the first elevated $\delta^{13}C$ value above this
613 unconformity. At first sight, this looks very straightforward: Munnecke and Männik (2009)
614 show the 184.95 m sample as being within the *D. staurognathoides* Biozone, 0.6 m below
615 the base of the *Pt. eopennatus* ssp. n. 1 Biozone. However, Männik (in Põldvere, 2010)
616 stated that the *D. staurognathoides* Biozone is “unidentifiable” in the Viki core “due to too
617 poorly represented faunas” and thus the change to abundant, high diversity conodont faunas
618 marking the base of the *Pt. eopennatus* ssp. n. 1 Biozone may simply reflect improved
619 preservation or a change to favourable environmental conditions rather than origination. A
620 very similar pattern is seen in the Valgu-1 section Männik (2008): here the *Pt. eopennatus*
621 ssp. n. 1 Biozone commences immediately above a discontinuity surface, again above strata
622 yielding an impoverished, stratigraphically undiagnostic fauna (incidentally, a similar scenario
623 is seen in Iowa, as recently documented by McAdams et al., 2017). So, it must be borne in
624 mind that the base of the *Pt. eopennatus* Superzone may not reflect the evolutionary first
625 appearance of *Pt. eopennatus* and that in other sections with a more complete conodont
626 record through the lower Telychian the FAD of *Pt. eopennatus* could be at a lower
627 stratigraphical level. Also, the similarity of the pattern of conodont appearance in the Viki
628 core to that in the Valgu-1 section, where this is shown to be above a stratigraphical gap,
629 and the recognition of multiple discontinuity surfaces above the “O” bentonite (but still within
630 the Rumba Formation) at other localities (e.g. at Päri, five discontinuity surfaces are
631 recorded within the upper Rumba Formation above the “O” bed; Kaljo and Einasto, 1996),
632 suggests that the existence of an additional stratigraphical gap in the Viki succession above
633 the “Rumba low” and “O” bentonite, but below the first elevated $\delta^{13}C$ value must be
634 considered to be a distinct possibility.

635 The purpose of this necessarily rather lengthy discussion is to draw attention to the
636 fact that, although the biostratigraphy and chemostratigraphy of the Kallholn section would
637 initially suggest that the twin peaked positive $\delta^{13}C$ excursion here is correlative with the
638 lowermost part of the positive excursion associated with the Valgu event, it is possible that
639 the Kallholn excursion is a distinct, additional, stratigraphically earlier phenomenon.

10. Conclusions

1. The Kallholn (N) section is of Llandovery age ranging from the *P. leptotheca* Biozone (middle Aeronian) through to the *S. crispus* Biozone (lower Telychian).
2. The section is a discontinuous record with a newly recognised unconformity between the *L. convolutus* and *St. halli* biozones. The absence of the *St. sedgwickii* Biozone is very likely to be the result of a time of non-deposition and erosion during a globally recognised major sea level fall.
3. The $\delta^{13}C_{org}$ curve for Kallholn (N) shows minor fluctuations throughout most of the section with a major double peaked positive excursion (of 2 ‰) in the upper *Sp. turriculatus* Biozone. Evidence presented herein strongly supports the argument that this is a new excursion (the Kallholn excursion) that has been identified at Kallholn rather than it being associated with the event representing the onset of the excursion associated with the “Valgu Event”.
4. It has not been possible to recognise the Osmundsberg K-bentonite with certainty in the Kallholn (N) section. Further geochemical analyses of bentonites are required. The geochemical similarity of demonstrably stratigraphically unrelated bentonites casts some doubt on previous correlations of the “O” bed in Estonia with the Osmundsberg K-bentonite.

Acknowledgments

We thank Jan Ove Ebbestad for providing very useful advice with regards to fieldwork in the Siljan region. The research of JF was supported by the Grant Agency of the Czech Republic (GACR grant No. 17-18120S).

Author contribution

Graptolite biostratigraphy was carried out by N.W. with supervision from D.K.L.

N.W. wrote the manuscript with support of D.K.L.

P.M. carried out the conodont extraction and identifications.

J.F. carried out the $\delta^{13}C_{org}$ analyses.

R.F.L. assisted N.W. and D.K.L. in the collection of the material in the field.

References

Baarli, G.B., Johnson, M.E., Antoshkina, A.I., 2003. Silurian stratigraphy and paleogeography of Baltica. New York State Museum Bulletin 493, 3–34.

Bancroft, A.M., Brunton, F.R., Kleffner, M.A., 2015. Silurian conodont biostratigraphy and carbon ($\delta^{13}C_{carb}$) isotope stratigraphy of the Victor Mine (V-03-270-AH) core in the Moose River Basin. Canadian Journal of Earth Sciences 52, 1169–1181.

Bates, D.E.B., Kirk, N.H., 1984. Autecology of Silurian graptoloids. Special Papers in Palaeontology 32, 121–139.

Bates, D.E.B., Kirk, N.H., 1992. The ultrastructure, mode of construction and functioning of a number of Llandovery ancorate diplograptid and retiolitid graptolites. Modern Geology 17, 1–270.

Bergström, S.M., Eriksson, M.E., Young, S.A., Widmark, E., 2012. Conodont biostratigraphy,

and $\delta^{13}C$ and $\delta^{34}S$ isotope chemostratigraphy, of the uppermost Ordovician and Lower Silurian at Osmundsberg, Dalarna, Sweden. GFF 134, 251–272.

Bergström, S.M., Huff, W.D., Kolata, D.R., 1998. The Lower Silurian Osmundsberg K-bentonite. Part 1: stratigraphic position, distribution and palaeogeographic significance. Geological Magazine 135, 1–13.

Bergström, S.M., Toprak, F.Ö., Huff, W.D., Mundil, R., 2008. Implications of a new, biostratigraphically well-controlled, radio-isotopic age for the lower Telychian Stage of the Llandovery Series (Lower Silurian, Sweden). Episodes 31, 309–314.

Brett, C.E., Boucot, A.J., Jones, B., 1993. Absolute depths of Silurian benthic assemblages. Lethaia 26, 25–40.

Buchardt, B., Nielsen, T., 1985. Carbon and oxygen isotope composition of Cambro-Silurian limestone and anthraconite from Bornholm: evidence for deep burial diagenesis. Bulletin of the Geological Society of Denmark 33, 415–435.

Cramer, B.D., Brett, C.E., Melchin, M.J., Männik, P., Kleffner, M.A., McLaughlin, P.I.,Loydell, D.K., Munnecke, A., Jeppsson, L., Corradini, C., Brunton, F.R., Saltzman, M.R., 2011. Revised correlation of Silurian Provincial Series of North America with global and regional chronostratigraphic units and $\delta^{13}C_{carb}$ chemostratigraphy. Lethaia 44, 185–202.

Ebbestad, J.O.R., Högström, A.E.S., Frisk, Å.M., Martma, T., Kaljo, D., Kröger, B., Pärnaste H., 2015. Terminal Ordovician stratigraphy of the Siljan district, Sweden. GFF 137, 36–56.

Epstein, A.G., Epstein, J.B., Harris, L.D., 1977. Conodont color alteration – an index to organic metamorphism. Geological Survey Professional Paper 995, 1–27.

723

724 Frýda, J., Štorch, P., 2014. Carbon isotope chemostratigraphy of the Llandovery in northern
725 peri-Gondwana: new data from the Barrandian area, Czech Republic. Estonian Journal of
726 Earth Sciences 63, 220–226.

727

728 Gouldey, J.C., Saltzman, M.R., Young, S.A., Kaljo, D., 2010. Strontium and carbon isotope
729 stratigraphy of the Llandovery (Early Silurian): implications for tectonics and weathering.
730 Palaeogeography, Palaeoclimatology, Palaeoecology 296, 264–275.

731

732 Grahn, Y., 1998. Lower Silurian (Llandovery–Middle Wenlock) Chitinozoa and
733 biostratigraphy of the mainland of Sweden. GFF 120, 273–283.

734

735 Hedberg, H.D., 1988. The 1740 description by Daniel Tilas of stratigraphy and petroleum
736 occurrence at Osmundsberg in the Siljan region of central Sweden. AAPG, Tulsa. 96 pp.

737

738 Huang, B., Baarli, B.G., Zhan, R.B., Rong, J.Y., 2016. A new early Silurian brachiopod
739 genus, *Thulatrypa*, from Norway and South China, and its palaeobiogeographical
740 significance. Alcheringa, 40, 83-97.

741

742 Huff, W.D., 2016. K-bentonites: A review. American Mineralogist 101, 43–70.

743

744 Huff, W.D., Bergström, S.M., Kolata, D.R., Sun, H., 1998. The Lower Silurian Osmundsberg
745 K-bentonite. Part II: mineralogy, geochemistry, chemostratigraphy and tectonomagmatic
746 significance. Geological Magazine 135, 15–26.

747

748 Hutt, J.E., 1975. The Llandovery graptolites of the English Lake District. Part 2. Monograph
749 of the Palaeontographical Society 129 (542), 57–137.

Inanli, F.O., Huff, W.D., Bergström, S.M., 2009. The lower Silurian (Llandovery) Osmundsberg K-bentonite in Baltoscandia and the British Isles: Chemical fingerprinting and regional correlation. GFF 131, 269–279.

Jeppsson, L., Anehus, R., 1995. A buffered formic acid technique for conodont extraction. Journal of Paleontology, 69, 790–794.

Jourdan, F., Reimold, W.U., Deutsch, A., 2012. Dating terrestrial impact structures. Elements 8, 49–53.

Kaljo, D., Einasto, R., 1996. Päri outcrop. In: Meidla, T., Puura, I., Nemliher, J., Raukas, A., Saarse, L. (Eds.). The Third Baltic Stratigraphical Conference abstracts, field guide. Institute of Geology, Tallinn, 107–108.

Kaljo, D., Martma, T., 2000. Carbon isotopic composition of Llandovery rocks (East Baltic Silurian) with environmental interpretation. Proceedings of the Estonian Academy of Sciences, Geology 49, 267–283.

Kaljo, D., Vingisaar, P., 1969. On the sequence of the Raikküla Stage in southernmost Estonia. Eesti NSV Teadvste Akadeemia, Toimetised, Keemia Geoloogia 18, 270–277.

Kiipli, T., Kallaste, T., 2002. Correlation of Telychian sections from shallow to deep sea facies in Estonia and Latvia based on sanidine composition of bentonites. Proceedings of the Estonian Academy of Sciences, Geology 51, 143–156.

Kiipli, T., Männik, P., Batchelor, R.A., Kiipli, E., Kallaste, T., Perens, H., 2001. Correlation of

777 Telychian (Silurian) altered volcanic ash beds in Estonia, Sweden and Norway. Norwegian
778 Journal of Geology 81, 179–194.
779
780 Kröger, B., Ebbestad, J.O.R., Lehnert, O., Ullmann, C.V., Korte, C., Frei, R., Rasmussen,
781 C.M.Ø., 2015. Subaerial speleothems and deep karst in central Sweden linked to Hirnantian
782 glaciations. Journal of the Geological Society 172, 349–356.
783
784 Lehnert, O., Meinhold, G., Bergström, S.M., Calner, M., Ebbestad, J.O.R., Egenhoff, S.,
785 Frisk, Å.M., Hannah, J.L., Högström, A.E.S., Huff, W.D., Juhlin, C., Maletz, J., Stein, H.J.,
786 Sturkell, E., Vandenbroucke, T.R.A., 2012. New Ordovician–Silurian drill cores from the
787 Siljan impact structure in central Sweden: an integral part of the Swedish Deep Drilling
788 Program. GFF 134, 87–98.
789
790 Loydell, D.K., 1990. On the type material of the Llandovery (Silurian) graptoloid *Monograptus*
791 *pseudobecki* Bouček and Přibyl, 1942 and the species' biostratigraphical importance.
792 Scottish Journal of Geology 26, 119–123.
793
794 Loydell, D.K., 1991a. Isolated graptolites from the Llandovery of Kallholen, Sweden.
795 Palaeontology 34, 671–693.
796
797 Loydell, D.K., 1991b. Dob's Linn – the type locality of the Telychian (Upper Llandovery)
798 *Rastrites maximus* Biozone? Newsletters on Stratigraphy 25, 155–161.
799
800 Loydell, D.K., 1998. Early Silurian sea-level changes. Geological Magazine 135, 447–471.
801
802 Loydell, D.K., Frýda, J., Gutiérrez-Marco, J.C., 2015. The Aeronian/Telychian (Llandovery,
803 Silurian) boundary, with particular reference to sections around the El Pintado reservoir,
804 Seville Province, Spain. Bulletin of Geosciences 90, 743–794.

Loydell, D.K., Kaljo, D., Männik, P., 1998. Integrated biostratigraphy of the lower Silurian of the Ohesaare core, Saaremaa, Estonia. Geological Magazine 135, 769–783.

Loydell, D.K., Maletz, J., 2002. Isolated '*Monograptus*' *gemmatus* from the Silurian of Osmundsberget, Sweden. GFF 124, 193–196.

Loydell, D.K., Maletz, J., 2004. The Silurian graptolite genera *Streptograptus* and *Pseudostreptograptus*. Journal of Systematic Palaeontology 2, 65–93.

Loydell, D.K., Maletz, J., 2009. Isolated graptolites from the *Lituigraptus convolutus* Biozone (Silurian, Llandovery) of Dalarna, Sweden. Palaeontology 52, 273–296.

Loydell, D.K., Männik, P., Nestor, V., 2003. Integrated biostratigraphy of the lower Silurian of the Aizpute-41 core, Latvia. Geological Magazine 140, 205–229.

Loydell, D.K., Nestor, V., Männik, P., 2010. Integrated biostratigraphy of the lower Silurian of the Kolka-54 core, Latvia. Geological Magazine 147, 253–280.

Lu, X., Kendall, B., Stein, H.J., Li, C., Hannah, J.L., Gordon, G.W., Ebbestad, J.O.R., 2017. Marine redox conditions during deposition of Late Ordovician and Early Silurian organic-rich mudrocks in the Siljan ring district, central Sweden. Chemical Geology 457, 75–94.

Maletz, J., 2003. Genetically controlled cortical tissue deposition in *Normalograptus scalaris* (Hisinger, 1837). Paläontologische Zeitschrift 77, 471–476.

Maletz, J., Reich, M., 1997. Radiolarians and sponge spicules from the *Spirograptus turriculatus* Zone (Llandovery, Silurian) of the Siljan district, Dalarna (Sweden). Greifswalder

Geowissenschaftliche Beiträge 4, 101–111.

Männik, P., 2007. Some comments on Telychian–early Sheinwoodian conodont faunas, events and stratigraphy. Acta Palaeontologica Sinica 46 (Suppl.), 305–310.

Männik, P., 2008. Conodont dating of some Telychian (Silurian) sections in Estonia. Estonian Journal of Earth Sciences 57, 156–169.

McAdams, N.E.B., Bancroft, A.M., Cramer, B.D., Witzke, B.J., 2017. Integrated carbon isotope and conodont biochemostratigraphy of the Silurian (Aeronian–Telychian) of the east-central Iowa Basin, Iowa, USA. Newsletters on Stratigraphy 50, 391–416.

McLaughlin, P.I., Emsbo, P., Brett, C.E., 2012. Beyond black shales: the sedimentary and stable isotope records of oceanic anoxic events in a dominantly oxic basin (Silurian; Appalachian Basin, USA). Palaeogeography, Palaeoclimatology, Palaeoecology 367–368, 153–177.

Melchin, M.J., Holmden, C., 2006. Carbon isotope chemostratigraphy of the Llandovery in Arctic Canada: implications for global correlation and sea-level change. GFF 128, 173–180.

Melchin, M.J., Sadler, P.M., Cramer, B.D., 2012. The Silurian Period. In: Gradstein, F.M., Ogg, J.G., Schmitz, M.D., Ogg, G.M. (Eds.), The geologic time scale 2012. Elsevier, Amsterdam, 525–558.

Morad, S., Eshete, M., 1990. Petrology, chemistry and diagenesis of calcite concretions in Silurian shales from central Sweden. Sedimentary Geology 66, 113–134.

Munnecke, A., Männik, P., 2009. New biostratigraphic and chemostratigraphic data from the

Chicotte Formation (Llandovery, Anticosti Island, Laurentia) compared with the Viki core (Estonia, Baltica). Estonian Journal of Earth Sciences 58, 159–169.

Noble, P.J., Maletz, J., 2000. Radiolaria from the Telychian (Llandovery, Early Silurian) of Dalarna, Sweden. Micropaleontology 46, 265–275.

Põldvere, A., (2010). Viki drill core. Estonian Geological Sections Bulletin 10, 1–56.

Raiswell, R., 1987. Non-steady state microbiological diagenesis and the origin of concretions and nodular limestones. In: Marshall, J.D. (Ed.), Diagenesis of sedimentary sequences. Geological Society, London, Special Publication 36, 41–54.

Reimold, W.U., Kelly, S.P., Sherlock, S.C., Henkel, H., Koeberl, C., 2005. Laser argon dating of melt breccias from the Siljan impact structure, Sweden: Implications for a possible relationship to Late Devonian extinction events. Meteoritics & Planetary Science 40, 591–607.

Štorch, P., 1994. Graptolite biostratigraphy of the lower Silurian (Llandovery and Wenlock) of Bohemia. Geological Journal 29, 137–165.

Štorch, P., 1998. Graptolites of the *Pribylograptus leptotheca* and *Lituigraptus convolutus* biozones of Tmaň (Silurian, Czech Republic). Journal of the Czech Geological Society 43, 209–272.

Štorch, P., Frýda, J., 2012. The late Aeronian graptolite *sedgwickii* Event, associated positive carbon isotope excursion and facies changes in the Prague Synform (Barrandian area, Bohemia). Geological Magazine 149, 1089–1106.

888

889 Sullivan, N.B., Brett, C.E., McLaughlin, P.I., Kleffner, M.A., Cramer, B.D., 2014. Correlation
890 of the Waco Member of the Alger Shale Formation (Silurian; Llandovery; Telychian) in east-
891 central Kentucky and south-central Ohio. GFF 136, 254–258.

892

893 Thorslund, P., Jaanusson, V., 1960. The Cambrian, Ordovician, and Silurian in
894 Västergötland, Närke, Dalarna, and Jämtland, central Sweden. International Geological
895 Congress, 21st Session, Guide to Excursions Nos 23 and C18. Geological Survey of
896 Sweden, 51 pp.

897

898 Tilas, D., 1740. Mineral-Historia öfwer Osmunds-berget uti Rättwiks Sochn och
899 ÖsterDalarne af Daniel Tilas. Swenska Wetenskaps Academiens Handlingar 1, 202–209.

900

901 Törnquist. S.L., 1874. Om Siljanstraktens paleozoiska formationsled. Öfversigt af Kongliga
902 Vetenskaps-Akademiens Förhandlingar 31(4), 3–39.

903

904 Törnquist, S.L., 1879. Några iakttangelser öfver Dalarnes graptolitskiffrar. Geologiska
905 Föreningens i Stockholm Förhandlingar 4, 446–457.

906

907 Törnquist, S.L., 1890. Undersöknigar öfver Siljansområdets graptoliter. I. Lunds Universitets
908 Årsskrift 26, 1–33.

909

910 Törnquist, S.L., 1892. Undersöknigar öfver Siljansområdets graptoliter. II. Lunds Universitets
911 Årsskrift 28, 1–47.

912

913 Törnquist, S.L., 1907. Observations on the genus *Rastrites* and some allied species of
914 *Monograptus.* Lunds Universitets Årsskrift (N.S.) 3(5), 1–22.

915

916 Torsvik, T.H., Cocks, L.R.M., 2013. New global palaeogeographical reconstructions for the
917 Early Palaeozoic and their generation. Geological Society, London, Memoirs 38, 5–24.
918
919 Umeda, M., Suzuki, Y., 2005. Aeronian (Llandovery, Early Silurian) radiolarians from the
920 Kallholn Formation in Siljan district, Sweden. Micropaleontology 51, 83-91.
921
922 Waid, C.B.T., Cramer, B.D., 2017. Global chronostratigraphic correlation of the Llandovery
923 Series (Silurian System) in Iowa, USA, using high-resolution carbon isotope ($\delta^{13}C_{carb}$)
924 chemostratigraphy and brachiopod and conodont biostratigraphy. Bulletin of Geosciences
925 92, 373–390.
926
927 Zalasiewicz, J., 1994. Middle to late Telychian (Silurian: Llandovery) graptolite assemblages
928 of central Wales. Palaeontology 37, 375–396.

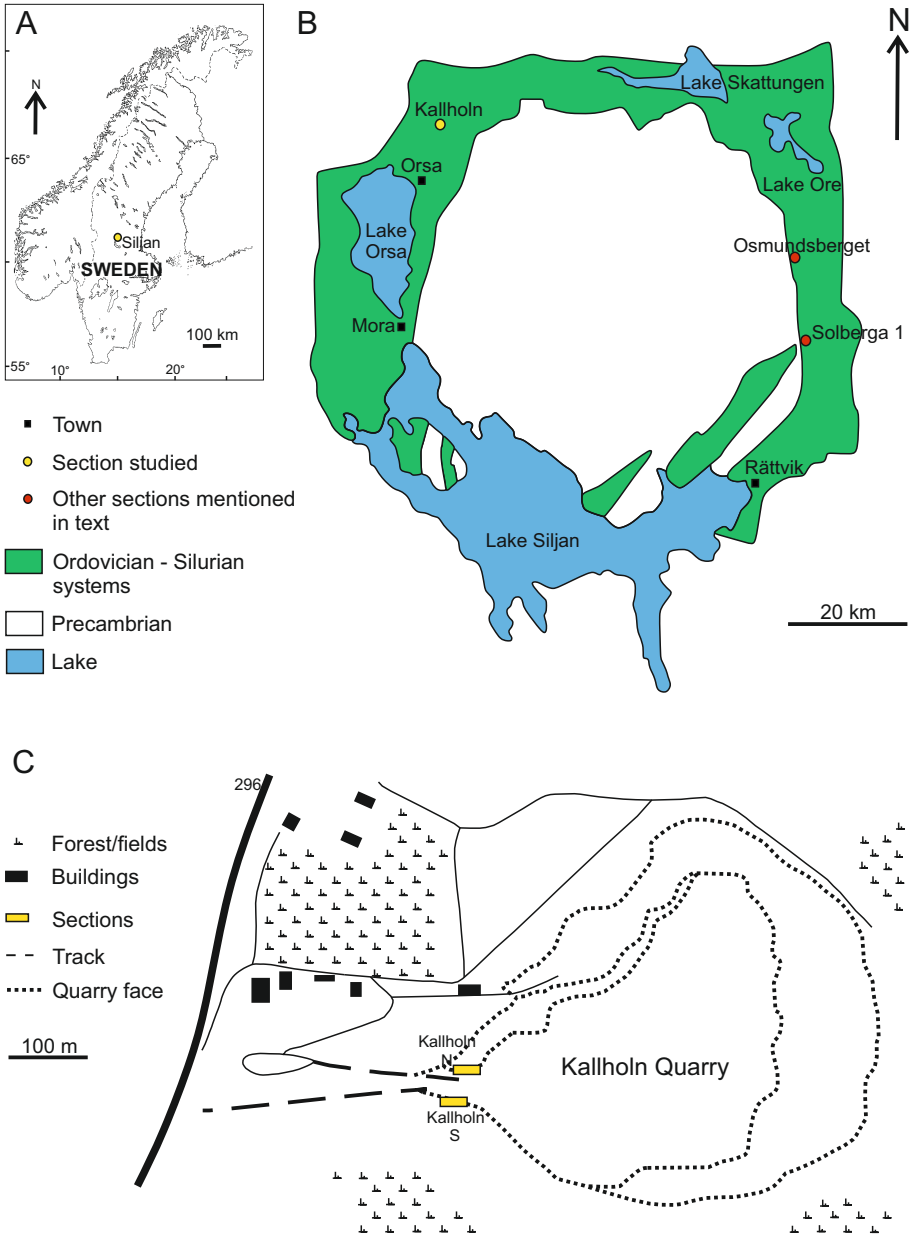
A
N
65°
Siljan
SWEDEN
100 km
55°
10°
20°
B
N
Kallholn
Lake Skattungen
Orsa
Lake Ore
Lake Orsa
Osmundsberget
Mora
Solberga 1
Rättvik
Lake Siljan
20 km
Town
Section studied
Other sections mentioned in text
Ordovician - Silurian systems
Precambrian
Lake
C
296
Forest/fields
Buildings
Sections
Track
Quarry face
100 m
Kallholn N
Kallholn Quarry
Kallholn S

Fig. 1

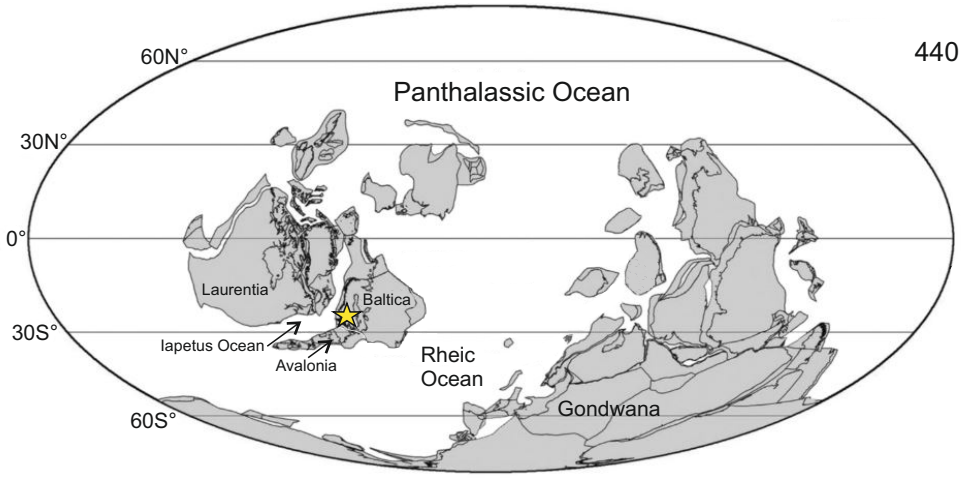
440 Ma
60N°
30N°
0°
30S°
60S°
Panthalassic Ocean
Laurentia
Baltica
Iapetus Ocean
Avalonia
Rheic
Ocean
Gondwana

Fig. 2

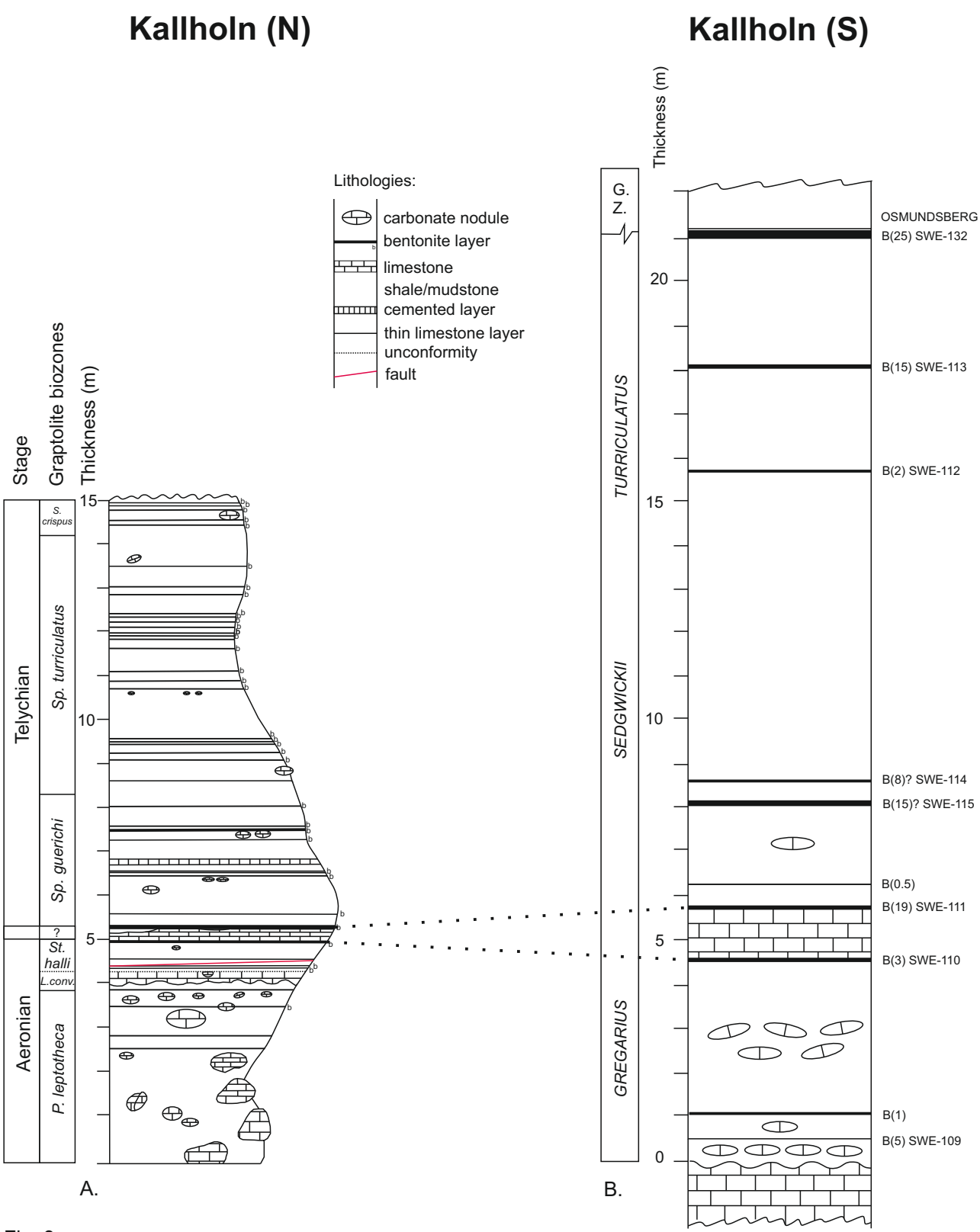
Kallholn (N)
Kallholn (S)
Lithologies:
carbonate nodule
bentonite layer
limestone
shale/mudstone
cemented layer
thin limestone layer
unconformity
fault
Stage
Graptolite biozones
Thickness (m)
Telychian
Aeronian
S. crispus
Sp. turriculatus
Sp. guerichi
?
St. halli
L.conv.
P. leptotheca
15
10
5
A.
G. Z.
TURRICULATUS
SEDGWICKII
GREGARIUS
Thickness (m)
20
15
10
5
0
OSMUNDSBERG
B(25) SWE-132
B(15) SWE-113
B(2) SWE-112
B(8)? SWE-114
B(15)? SWE-115
B(0.5)
B(19) SWE-111
B(3) SWE-110
B(1)
B(5) SWE-109
B.

Fig. 3

A

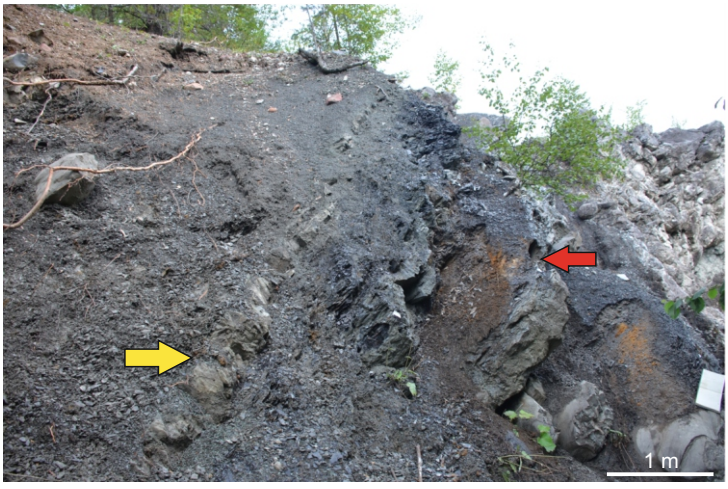

B

C

D

E

F

Fig. 4

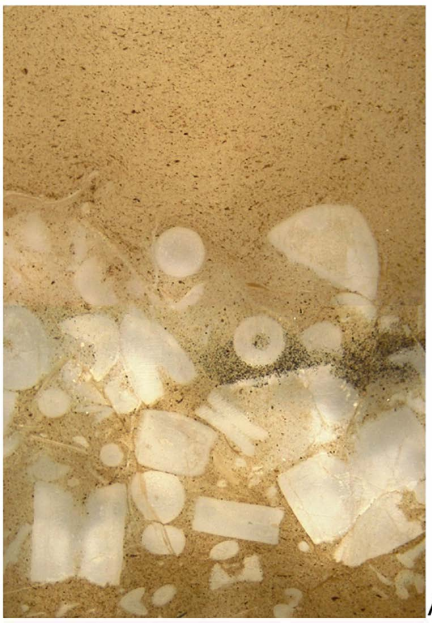
A


B


G

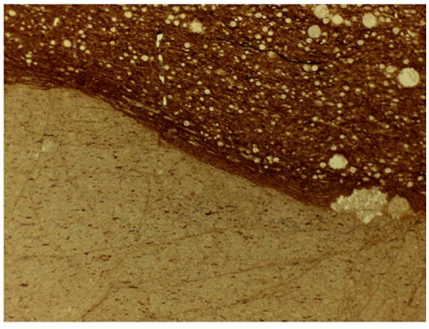
C


F


D


E

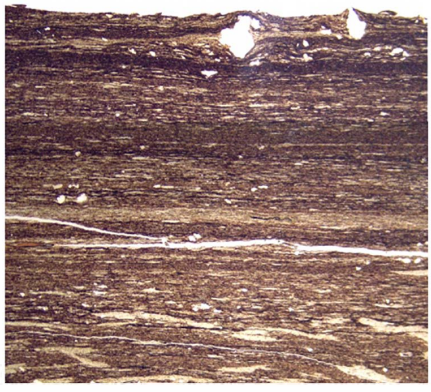
H

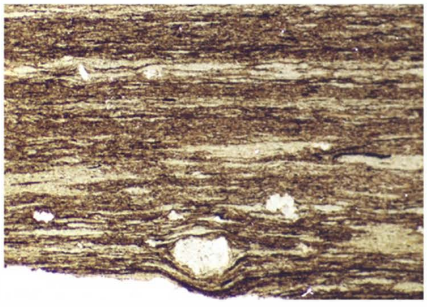
I

Fig. 5

Fig. 6

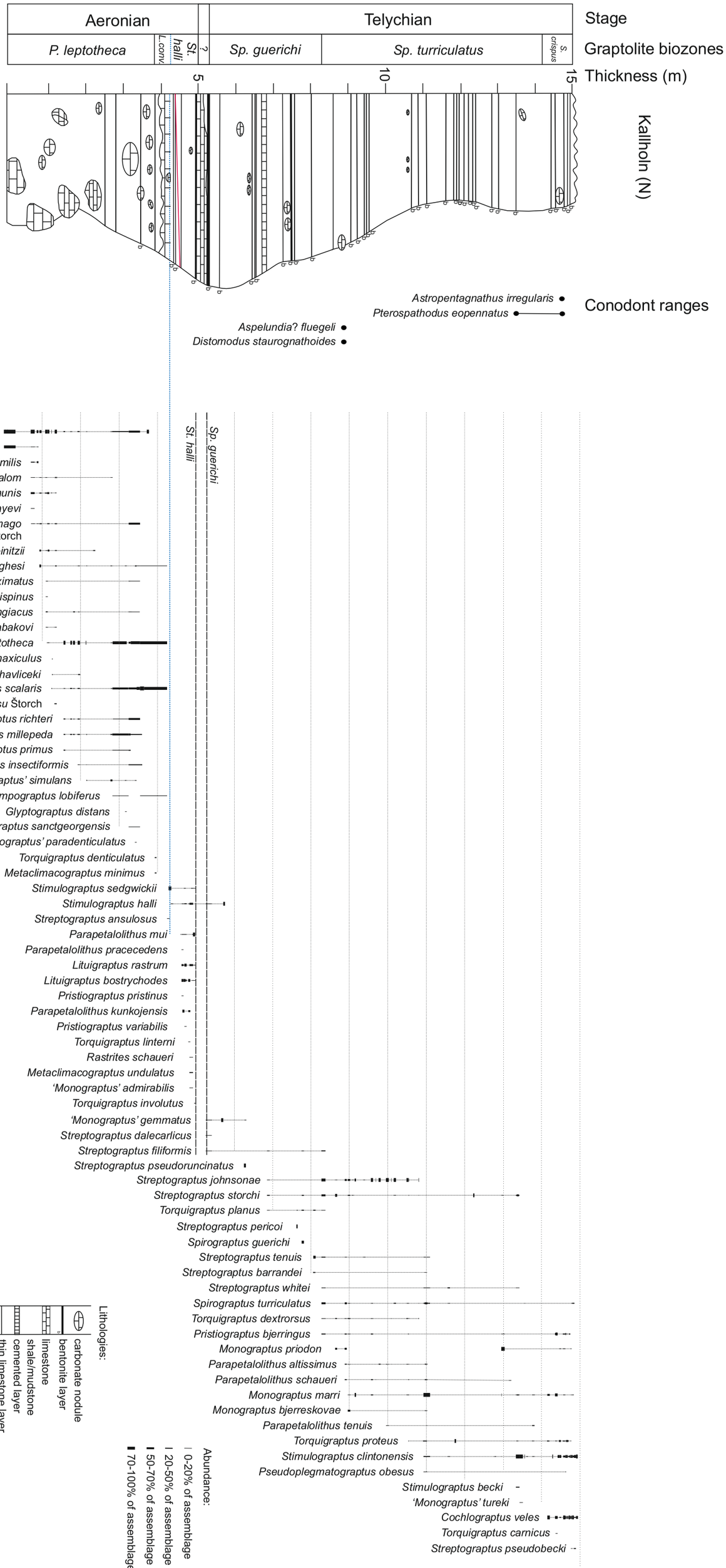
Aeronian
Telychian
Stage
P. leptotheca
L.conv.
St. halli
?
Sp. guerichi
Sp. turriculatus
S. crispus
Graptolite biozones
5
10
15
Thickness (m)
Kallholn (N)
Astropentagnathus irregularis
Pterospathodus eopennatus
Aspelundia? fluegeli
Distomodus staurognathoides
Conodont ranges
St. halli
Sp. guerichi
Coronograptus gregarius
Pristiograptus fragilis
Demirastrites similis
Metaclimacograptus slalom
Campograptus communis
Korenograptus nikolayevi
Monoclimacograptus aff. imago sensu Štorch
Rastrites geinitzii
Metaclimacograptus hughesi
Rastrites approximatus
Rastrites longispinus
Rickardsograptus thuringiacus
Metaclimacograptus khabakovi
Pribylograptus leptotheca
Coronograptus maxiculus
'Monograptus' havliceki
Normalograptus scalaris
Petalolithus aff. ovatoelongatus sensu Štorch
Lituigraptus richteri
Campograptus millepeda
Agetograptus primus
Pseudorthograptus insectiformis
'Monograptus' simulans
Campograptus lobiferus
Glyptograptus distans
Campograptus sanctgeorgensis
'Monograptus' paradenticulatus
Torquigraptus denticulatus
Metaclimacograptus minimus
Stimulograptus sedgwickii
Stimulograptus halli
Streptograptus ansulosus
Parapetalolithus mui
Parapetalolithus pracecedens
Lituigraptus rastrum
Lituigraptus bostrychodes
Pristiograptus pristinus
Parapetalolithus kunkojensis
Pristiograptus variabilis
Torquigraptus linterni
Rastrites schaueri
Metaclimacograptus undulatus
'Monograptus' admirabilis
Torquigraptus involutus
'Monograptus' gemmatus
Streptograptus dalecarlicus
Streptograptus filiformis
Streptograptus pseudoruncinatus
Streptograptus johnsonae
Streptograptus storchi
Torquigraptus planus
Streptograptus pericoi
Spirograptus guerichi
Streptograptus tenuis
Streptograptus barrandei
Streptograptus whitei
Spirograptus turriculatus
Torquigraptus dextrorsus
Pristiograptus bjerringus
Monograptus priodon
Parapetalolithus altissimus
Parapetalolithus schaueri
Monograptus marri
Monograptus bjerreskovae
Parapetalolithus tenuis
Torquigraptus proteus
Stimulograptus clintonensis
Pseudoplegmatograptus obesus
Stimulograptus becki
'Monograptus' tureki
Cochlograptus veles
Torquigraptus carnicus
Streptograptus pseudobecki
Lithologies:
carbonate nodule
bentonite layer
limestone
shale/mudstone
cemented layer
thin limestone layer
unconformity
fault
Abundance:
0-20% of assemblage
20-50% of assemblage
50-70% of assemblage
70-100% of assemblage

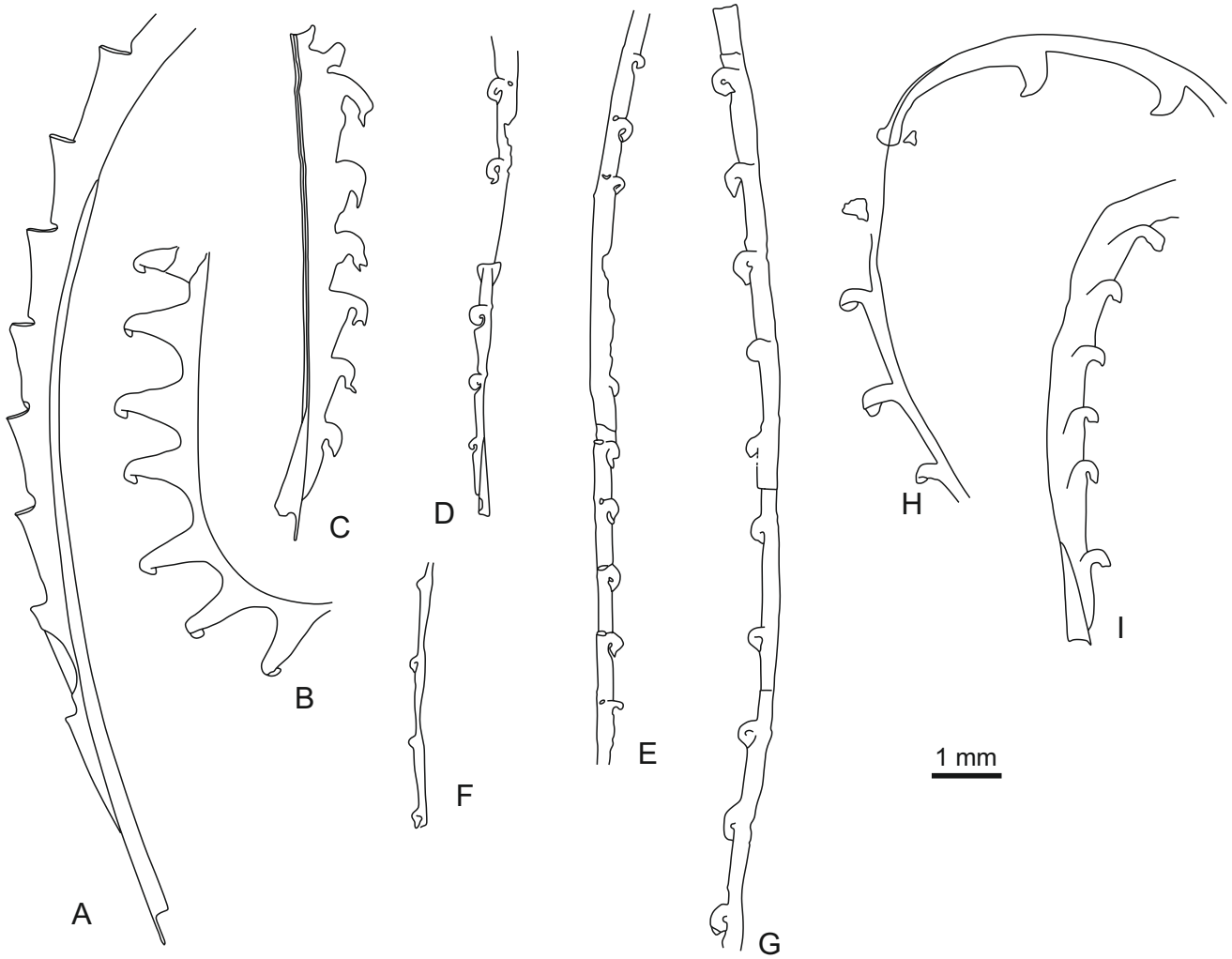

Fig. 7

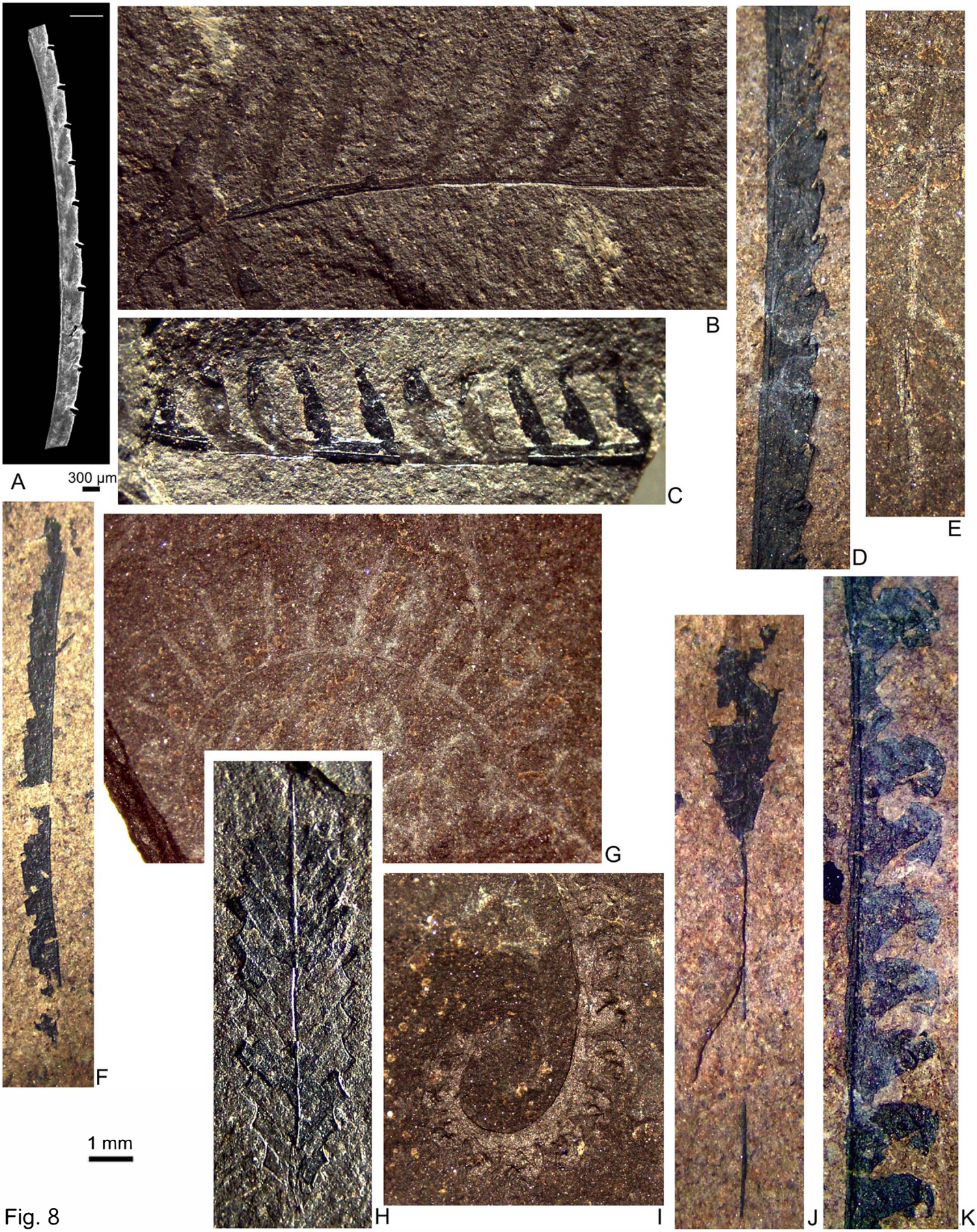

Fig. 8

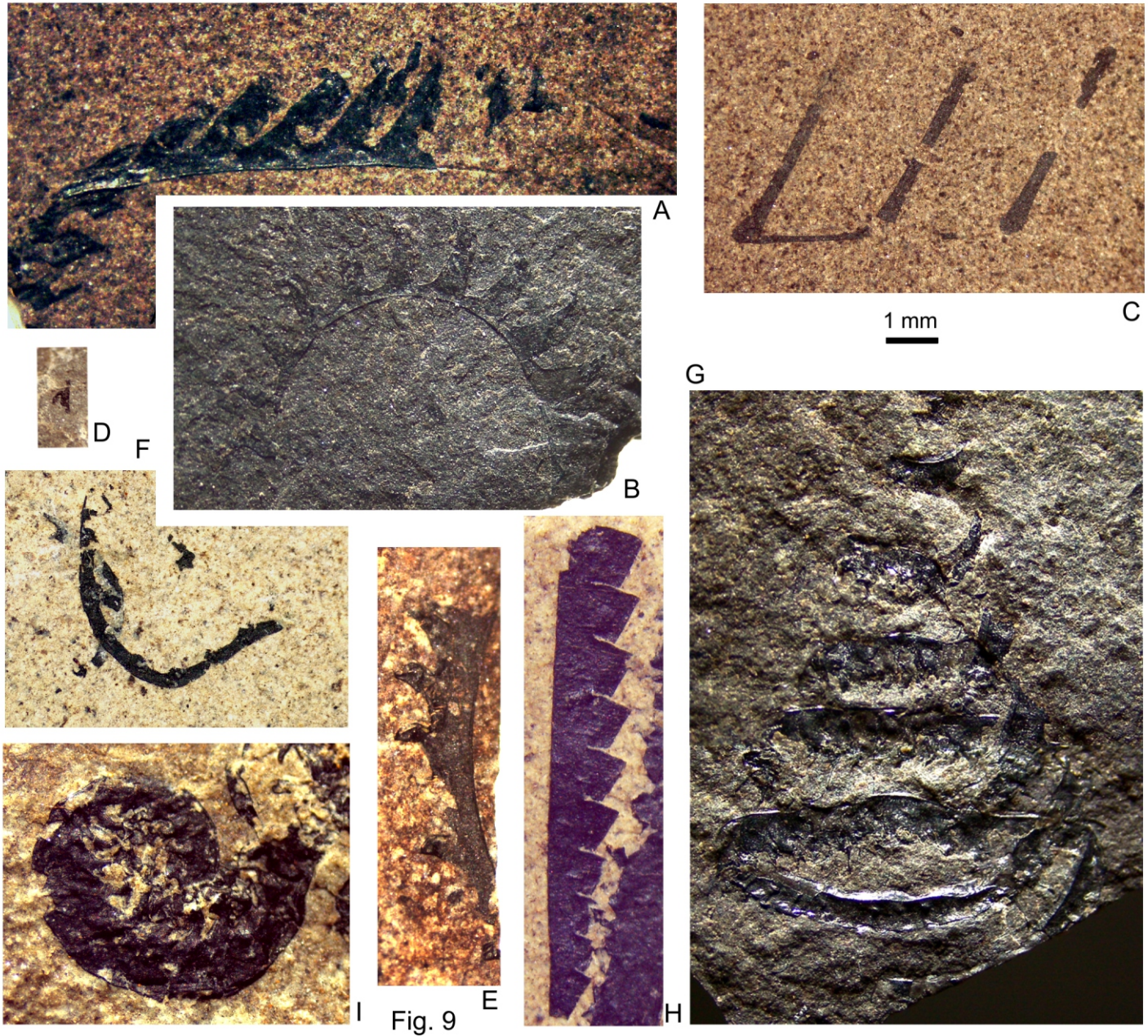

Fig. 9

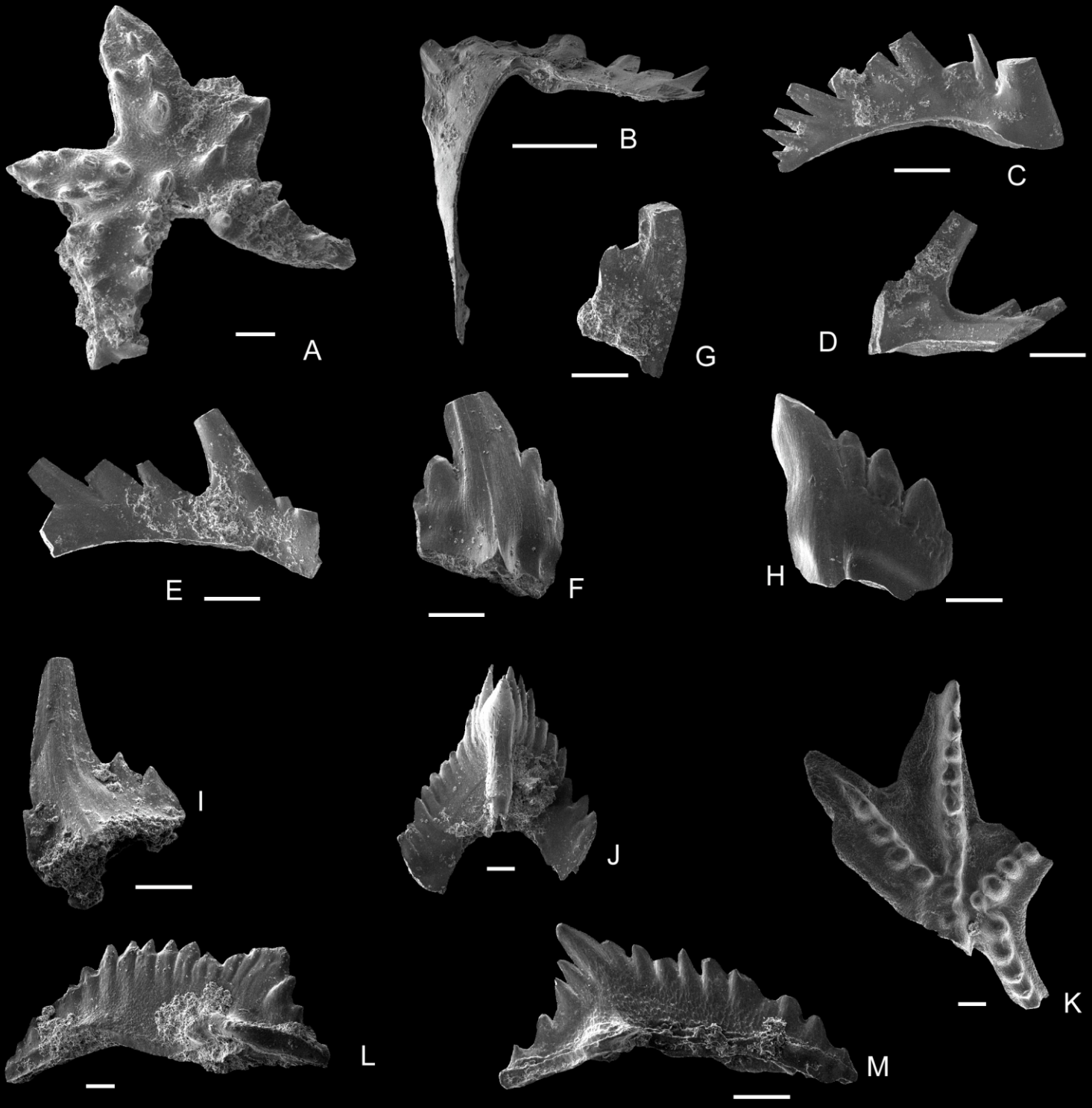

Fig. 10

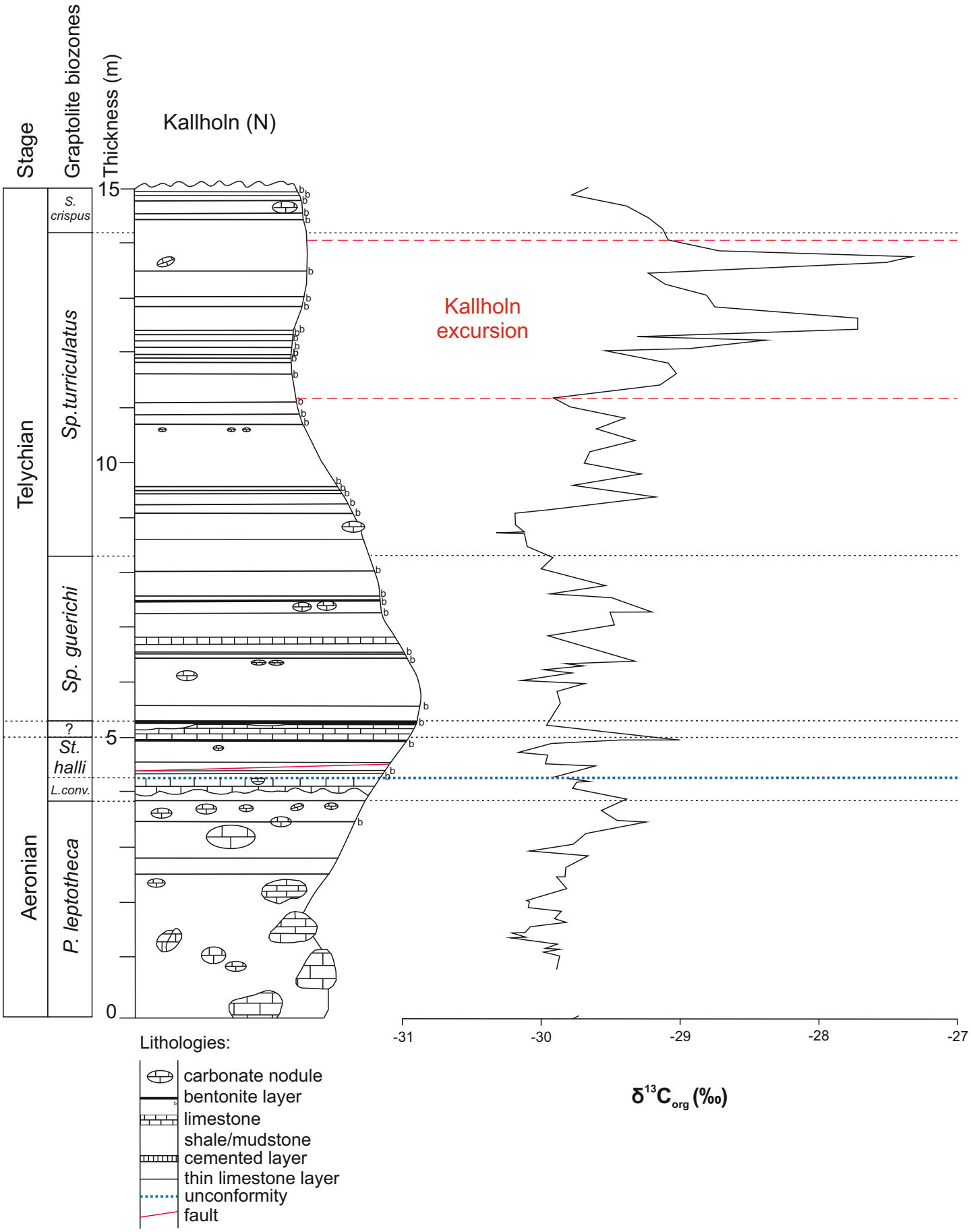
Stage
Graptolite biozones
Thickness (m)
Kallholn (N)
Telychian
Aeronian
S. crispus
Sp.turriculatus
Sp. guerichi
?
St. halli
L.conv.
P. leptotheca
15
10
5
0
Kallholn excursion
-31
-30
-29
-28
-27
δ13Corg (‰)
Lithologies:
carbonate nodule
bentonite layer
limestone
shale/mudstone
cemented layer
thin limestone layer
unconformity
fault

Fig. 11

Sample height	$\delta^{13}C_{org}$ (‰)	Lithology
0-0.05	-29.78	nodule
0.04-0.13	-29.74	nodule
0.93-0.98	-29.88	black shale
1.13-1.18	-29.87	black shale
1.20	-29.98	nodule
1.25	-29.87	black shale
1.25	-29.97	nodule
1.33-1.38	-29.89	black shale
1.45-1.52	-30.21	nodule
1.45-1.52	-30.11	nodule
1.53-1.58	-30.20	black shale
1.55-1.60	-30.121	black shale
1.65	-30.08	black shale
1.73-1.78	-29.84	black shale
1.80-1.85	-29.89	black shale
1.93-1.98	-29.86	black shale
2.00	-30.09	nodule
2.13-2.18	-30.08	black shale
2.13-2.18	-30.10	nodule
2.33-2.38	-29.82	black shale
2.55-2.58	-29.89	black shale
2.55-2.60	-29.83	black shale
2.73-2.78	-29.83	black shale
2.93-2.98	-29.66	black shale
3.01	-30.08	nodule
3.13-3.18	-29.77	shale
3.33-3.38	-29.68	black shale
3.53-3.58	-29.25	shale
3.56	-29.46	nodule
3.73-3.78	-29.57	black shale
3.93-3.98	-29.38	black shale
4.13-4.20	-29.78	nodule
4.26	-29.74	nodule
4.26-4.31	-29.65	black shale
4.34-4.44	-29.89	black shale
4.53-4.57	-29.62	black shale
4.57-4.58	-29.96	black shale
4.73-4.78	-29.95	black shale
4.78-4.83	-30.16	black shale
4.93-4.98	-29.93	black shale
5.05	-29.43	limestone
5.10	-29.06	limestone
5.15	-29.01	limestone

5.26-5.31	-29.97	shale
5.46-5.51	-29.92	shale
5.66-5.71	-29.86	shale
5.86-5.91	-29.89	shale
6.01-6.21	-29.69	nodule
6.06-6.11	-30.13	shale
6.20-6.22	-29.79	shale
6.26-6.31	-29.98	shale
6.36	-29.68	nodule
6.36	-29.82	shale
6.41-6.46	-29.34	shale
6.86-6.91	-29.95	black shale
7.06-7.11	-29.47	shale
7.29	-29.50	nodule
7.29	-29.22	nodule
7.55	-29.50	nodule
7.62-7.66	-29.92	black shale
7.76-7.81	-29.54	black shale
8.06-8.11	-29.99	black shale
8.26-8.31	-29.92	black shale
8.46-8.51	-30.10	black shale
8.66-8.71	-30.12	black shale
8.70	-30.12	black shale
8.70	-30.12	nodule
8.71-8.77	-30.31	black shale
8.86-8.91	-30.18	black shale
9.06-9.11	-30.19	black shale
9.13-9.17	-29.94	black shale
9.26-9.31	-29.48	black shale
9.36-9.41	-29.18	black shale
9.56-9.61	-29.77	black shale
9.76-9.81	-29.28	black shale
9.96-10.01	-29.69	black shale
10.16-10.21	-29.65	black shale
10.36-10.41	-29.33	black shale
10.56-10.61	-29.61	black shale
10.76-10.81	-29.40	black shale
10.96-11.01	-29.79	black shale
11.13-11.18	-29.91	black shale
11.36-11.41	-29.15	black shale
11.56-11.61	-29.03	black shale
11.745-11.795	-29.09	black shale
11.97-12.01	-29.53	black shale
12.01-12.07	-28.93	black shale
12.16-12.21	-28.39	black shale

12.22-12.26	-29.30	black shale
12.36-12.41	-27.72	black shale
12.56-12.61	-27.72	black shale
12.76-12.81	-28.75	black shale
12.96-13.01	-28.81	black shale
13.16-13.21	-29.11	black shale
13.36-13.41	-29.23	black shale
13.56-13.61	-27.51	nodule
13.66	-27.33	nodule
13.76-13.81	-28.72	black shale
13.96-14.01	-29.08	black shale
14.16-14.21	-29.12	shale
14.36-14.41	-29.23	black shale
14.56-14.61	-29.39	black shale
14.61	-29.56	nodule
14.76-14.81	-29.78	black shale
14.85	-29.64	nodule
14.90-14.95	-29.66	black shale

Fig. 1. A. Map of Sweden showing the location of the Siljan impact crater. B. A simplified geological map of the Siljan area showing the location of Kallholn and other localities mentioned in the text. Maps modified from Loydell and Maletz (2002) and Umeda and Suzuki (2005). C. Map of the Kallholn quarry showing the location of the section studied herein, Kallholn (N), and the section studied by Bergström et al. (1998), Kallholn (S). Map modified from Ebbestad et al. (2015).

Fig. 2. Global palaeogeography for the early Silurian Period, Llandovery Epoch, modified from Huang et al. (2016). The location of Kallholn is marked with a yellow star.

Fig. 3. Comparison of sedimentary logs and graptolite biozonations for the Kallholn sections. A. Log and graptolite biozonation of the Kallholn (N) section generated during the present study (b = bentonites). B. Log of the Kallholn (S) section (B = bentonites) from Bergström et al. (1998) and Inanli et al. (2009).

Fig. 4. Kallholn quarry field photographs. A. Overview of the lower part of the Kallholn (N) section studied. B. Part of the Kallholn (N) section showing the marker limestone bed with its base at 5.0 m (yellow arrow points to top of this limestone) and unconformity between the *L. convolutus* and *St. halli* biozones at 4.26 m (red arrow). C. Highest part of the section after excavation, showing large nodules with bases at 13.66 m and 14.61 m. D. Lowest part of the Kallholn (N) section studied, showing the unconformity between the Upper Ordovician Boda Limestone and the shales of the Aeronian Kallholn Formation. E. Bentonite (marked by the blue arrow) in the upper part (lower Telychian) of the Kallholn (N) section interbedded with dark green shales and darker graptolitic shales. F. Karstic fissures within the Ordovician Boda Limestone mound at east end of Kallholn quarry, infilled by darker Silurian (Aeronian) graptolitic shale.

Fig. 5. Key beds and some lithological features within the Kallholn (N) section. A. Thin section of crinoidal limestone, a useful marker bed, at 3.86 m. B–D. Unconformity at 4.26 m between the *L. convolutus* and *St. halli* biozones, at the top of the planed-off carbonate nodule. B, C, thin sections; note irregular nature to top of nodule, truncation of poorly developed laminations within carbonate at top of nodule, possible encrusters on unconformity surface (?hardground on sea floor) and abundant radiolarians in shale above unconformity; D, hand specimen from which thin section was taken. E. Thin section of bioclastic limestone (a packstone), which forms a useful marker bed (at 4.57 m) within the *St. halli* Biozone and can be recognised also in the Kallholn (S) section. F. Cone-in-cone structures at 11.79 m. G. Thin section of the carbonate nodule at 13.66 m; note recrystallization of micrite to microspar in lower part and burrows within laminated upper part (horizontal lines within this figure are image joins). H, I. Thin section of laminated shales (with *Chondrites* at base of h) at 10.96 m. Scale bars represent 1 mm.

Fig. 6. Conodont occurrences and range chart of graptolites in the Kallholn (N) section. Scale is in metres. *P. = Pribylograptus*; *L. conv. = Lituigraptus convolutus*; *St. = Stimulograptus*; *Sp. = Spirograptus*; S. = *Streptograptus*.

Fig. 7. Graptolites from the Kallholn (N) section. A. *Coronograptus gregarius* (Lapworth), *P. leptotheca* Biozone, PMU 31786, 3.41–3.46 m. B. *Torquigraptus denticulatus* (Törnquist), *L. convolutus* Biozone, PMU 31795, 3.93–3.98 m. C. *Stimulograptus halli* (Barrande), *St. halli* Biozone, PMU 31776, 4.26–4.31 m. D. *Streptograptus dalecarlicus* Loydell and Maletz, *Sp. guerichi* Biozone, PMU 31794, 5.26–5.41 m. E. *Streptograptus pericoi* Štorch, *Sp. guerichi* Biozone, PMU 31796, 7.62–7.66 m. F. *Streptograptus tenuis* Loydell, *Sp. turriculatus* Biozone, PMU 31783, 14.79–14.80 m. G. *Streptograptus whitei* Zalasiewicz, *Sp. turriculatus*

Biozone, PMU 31797, 8.29–8.39 m. H. *Torquigraptus proteus* (Barrande), *Sp. turriculatus* Biozone, PMU 31798, 10.96–11.01 m. I. *'Monograptus' tureki* Štorch, *Sp. turriculatus* Biozone, PMU 31780, 13.42–13.51 m. Scale bar represents 1 mm.

Fig. 8. Graptolites from the Kallholn (N) section. A. *'Monograptus'* aff*. imago* sensu Štorch, *P. leptotheca* Biozone, PMU 31800, specimen chemically isolated from limestone nodule at 1.25 m. B. *Rastrites approximatus* Perner, *P.* leptotheca Biozone, PMU 31788, 1.09–1.14 m. C. *Lituigraptus richteri* (Perner), *P. leptotheca* Biozone, PMU 31792, 1.56–1.60 m. D. *Pribylograptus leptotheca* (Lapworth), *P. leptotheca* Biozone, PMU 31772, 3.25–3.30 m. E. *Coronograptus maxiculus* Štorch, *P. leptotheca* Biozone, PMU 31791, 1.25 m. F. *'Monograptus' havliceki* Štorch, *P. leptotheca* Biozone, PMU 31784, 1.93–1.98 m. G. *Rastrites longispinus* Perner, *P. leptotheca* Biozone, PMU 31793, 1.09–1.14 m. H. *Parapetalolithus mui* Loydell, Frýda and Gutiérrez-Marco, *St. halli* Biozone, PMU 31790, 4.63–4.68 m. I. *Campograptus millepeda* (McCoy), *P. leptotheca* Biozone, PMU 31787, 2.15-2.17 m. J. *Agetograptus primus* Obut and Sobolevskaya, *P. leptotheca* Biozone, PMU 31773, 3.25–3.30 m. K. *Campograptus lobiferus* (McCoy), *P. leptotheca* Biozone, PMU 31785, 2.83–3.24 m. Scale bar represents 1 mm (B-K) and 300 μm (A).

Fig. 9. Graptolites from the Kallholn (N) section. A. *Lituigraptus rastrum* (Richter), *St. halli* Biozone, PMU 31782, 4.70–4.75 m. B. *Rastrites schaueri* Štorch and Loydell, *St. halli* Biozone, PMU 31781, 4.83–4.93 m. C. '*Monograptus' gemmatus* (Barrande), *Sp. guerichi* Biozone, PMU 31778, 5.66–5.71 m. D. *Lituigraptus bostrychodes* Loydell, Frýda and Gutiérrez-Marco, *St. halli* Biozone, PMU 31789, 4.80–4.85 m. E. *Streptograptus johnsonae* Loydell, *Sp. turriculatus* Biozone, PMU 31770, 10.54 m. F. *Cochlograptus veles* (Richter), *S. crispus* Biozone, PMU 31771, 14.90–14.95 m. G. *Torquigraptus planus* (Barrande), *Sp. guerichi* Biozone, PMU 31779, 7.62–7.66 m. H. *Pristiograptus bjerringus* (Bjerreskov), *Sp.*

turriculatus Biozone, PMU 31775, 10.54 m. I. *Spirograptus turriculatus* (Barrande), *Sp. turriculatus* Biozone, PMU 31799, 8.97–9.02 m. Scale bars represent 1 mm.

Fig. 10. Selected conodonts from the Kallholn (N) section. A. *Distomodus staurognathoides* (Walliser), Pa element, GIT 793-1, sample 8.70–8.80 m. B, C. *Oulodus*? sp. (B) Sc element, GIT 793-2; (C) Pa element, GIT 793-3. Both elements from sample 8.70–8.80 m. D–G. *Aspelundia*? *fluegeli* (Walliser). (D) Pa element, GIT 793-4; (E) M element, GIT 793-5; (F) Pb element, GIT 793-6; (G) Sc element, GIT 793-7. All elements from sample 8.70–8.80 m. H, I. *Dapsilodus* sp. (H) high-based slightly asymmetrical element, GIT 793-8; (I) low-based element GIT 793-9. Both elements from sample 8.70–8.80 m. J, M, N, R. *Pterospathodus eopennatus* Männik. (J) Pc? element, GIT 793-10; (M) Sc_2 element, GIT 793-11; (N) Pb_1 element, GIT 793-12; (R) Pc element, GIT 793-13. J, M, N from sample 13.66–13.91 m; R from sample 14.73–14.82 m. K, Q, S, T. *Astropentagnathus irregularis* Mostler. (K) Sa element, GIT 793-14; (Q) Pa_1 element, GIT 793-15; (S, T) Pb elements, GIT 793-16 and GIT 793-17. K and S from sample 14.76–14.95 m; Q and T from sample 14.73–14. 82 m. L, O, P. *Dapsilodus* aff. *sparsus* Barrick. (L). High-based slightly asymmetrical element, GIT 793-18; (O) high-based symmetrical element, GIT 793-19; (P) low-based element, GIT 793-20. L from sample 13.66–13.91 m, O from sample 14.76–14.95 m and P from sample 14.73–14.82 m. Scale bar represents 100 µm.

Fig. 11. The $\delta^{13}C_{org}$ record through the Kallholn (N) section. Vertical scale is in metres.